Oblique, Stratified Winds about a Shelter Fence. Part II: Comparison of Measurements with Numerical Models

JOHN D. WILSON

Department of Earth and Atmospheric Sciences, University of Alberta, Edmonton, Alberta, Canada

(Manuscript received 23 September 2003, in final form 9 April 2004)

ABSTRACT

To evaluate Reynolds-averaged Navier–Stokes (RANS) models of disturbed micrometeorological winds, steady-state computations using a second-order closure are compared with observations (see Part I) in which the surface layer wind was disturbed by a long, thin porous fence (height $h = 1.25$ m; thickness $d_x \approx 1$ mm). Starting with the case of neutral stratification and normal incidence, it is shown that low-resolution RANS simulations (streamwise grid interval $\Delta x/h = 1$) produce reasonably good transects of mean wind speed, though with an ambiguity (or nonuniqueness) of at least 10%–15% of the amplitude of the relative wind curve, mainly arising from sensitivity to the choice of the solution mesh. For nearly perpendicular flows, the measured influence of stratification (stable or unstable) is to diminish the amplitude of the relative wind curve (i.e., windbreak is *less* effective), an effect that is replicated very well by the simulations. Obliquity of the incident wind, like stratification, also correlates with poorer shelter, but the computed response of the relative wind curve to obliquity is excessive. As for higher-order wind statistics, computed transects of velocity standard deviations compare poorly to those observed. Therefore, if this disturbed flow may be taken as representative, then caution must be recommended should it be thought that RANS-type models might be suitable (i.e., accurate, as well as convenient) for computing the disturbed wind statistics (typically mean velocity, shear stress tensor, and turbulent kinetic energy dissipation rate) that are needed to ''drive'' modern dispersion models in the complex wind regimes that must be confronted in such contexts as urban dispersion, or the wind migration of pollen.

1. Introduction

The disturbance to the mean winds engendered by a long, straight windbreak presents a well-defined, two-dimensional flow that, like the step change in surface temperature or surface roughness, is a useful diagnostic for the generality of our understanding of micrometeorology, and more specifically for computational fluid mechanics. Although there might be some practical value to a capacity to confidently and accurately model shelter flows, perhaps the greater importance of shelter simulations lies in what we can learn from them of the viability and objectivity of computational fluid mechanics, which has assumed an influential role in society regarding environmental planning and regulation.

The aim of this paper is to establish whether the disappointing performance of steady-state Reynolds-averaged Navier–Stokes (RANS) models for the simulation of neutral winds about multiple parallel shelter fences was an anomaly, or whether we indeed have ''bumped against a boundary, between the do-able and the not do-able, for RANS models, in micro-meteorology'' (Wilson and Yee 2003). New simulations, using RANS models with second-order closure, will be compared with the observations of Wilson (2004, hereinafter Part I), wherein a stratified surface layer encountered a long fence at oblique incidence. Although it has been shown (Wilson 1985, hereinafter W85; Wang and Takle 1995b) that neutral winds at perpendicular incidence are simulated quite well even by first-order closures, the present observations address the effects of the stability and obliquity of incidence.

Simulations of this paper are distinct from the oblique windbreak computations of Wang and Takle (1996) in several respects: Wang and Takle considered windbreaks of finite width, only in the neutral case, and used a single eddy viscosity (K) closure. Tailoring a first-order closure to account for stratification offers certain perplexities, which admittedly could be overcome, but at the outset it was decided instead to here examine second-order closures, on the principle that the role of stratification thereby enters more naturally. Second-order closures ''are calibrated against certain test situations, just like the first-order models, so we can be assured that approximately the correct amounts of momentum, heat, etc. are being transported'' (Lumley 1979). In principle, because they make no presupposition that the mean momentum flux must run down the mean velocity gradient,

Corresponding author address: John D. Wilson, Department of Earth and Atmospheric Sciences, University of Alberta, Edmonton, Alberta T6G 2E3, Canada.
E-mail: jaydee.uu@ualberta.ca

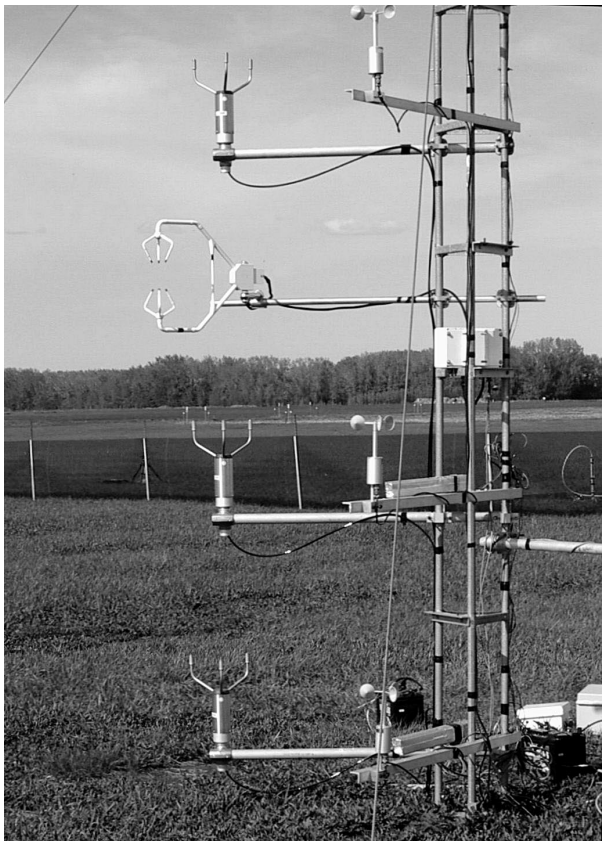

FIG. 1. Ellerslie, AB, Canada, windbreak experiment (spring, 2003). A view to the northeast showing the plastic fence (height $h = 1.25$ m), a three-dimensional sonic anemometer (centered at $z = 2$ m), paired cup and 2D sonic anemometers, and thermometer intake shields. Periods with winds approaching the tower from this direction were discarded.

they have a wider span of applicability than *K* closures, and indeed Launder's (1989) assessment was that ''second-moment closure offers a far more reliable approach to predicting complex flows than any eddy-viscosity-based model.'' Earlier opinion had not always been so positive (e.g., Lumley 1989, loc. cit.: ''it is usually found that the results . . . are not a substantial improvement'' over simulations using *K* theory).

Before looking at one-dimensional solutions (equilibrium vertical profiles for undisturbed flow) and windbreak simulations, formulation of the second-order closure model and the numerical method used for its solution will be covered. Because the closure assumptions are well known, emphasis will be placed on the novel aspects, that is, parameterization of the drag of the fence in oblique winds and formulation of the equations in a coordinate system in which orientation of the mean wind is arbitrary.

2. RANS computational wind models

The experimental shelter flow (Figs. 1 and 2) involved a straight, 45% porous plastic fence of height $h = 1.25$ m and length $Y = 114$ m, exposed on a uniform plain of grass (mean roughness length $z_0 = 0.019$ m). The resistance coefficient of the fence, deduced from the pressure drop observed across a section of the material that had been mounted so as to block a uniform wind tunnel stream, was $k_{r0} = 2.4$.

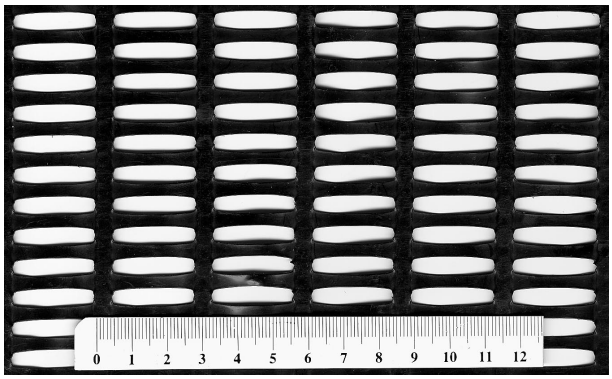

FIG. 2. A cut-out sample of the Tensar plastic windbreak. Scale is numbered in centimeters, and the semimajor axis of the pores measures about 2.3 cm. In field use the semimajor axis is parallel to ground.

The numerical simulations treat this windbreak flow as occurring within (i.e., disturbing) a constant stress layer, and assume a unidirectional approach flow satisfying the assumptions of the Monin–Obukhov similarity theory (MOST). The (modeled) fence will be assumed to be infinitely long, rigid, and oriented parallel to the *y* coordinate. Flow statistics are assumed to be independent of *y*; thus, although the simulations involve all three mean velocity components (*U*, *V*, *W*), these vary only along two space dimensions (two-dimensional simulations). The component *U* will always be perpendicular to the fence; thus, the numerical models must be formulated such that *both* mean horizontal velocity components may be nonzero upwind. A mean wind perpendicular to the fence will (herein) be denoted $\beta = 0$.

a. Averaging

It has been acknowledged since Wilson and Shaw (1977) that if the winds in a multiply connected space, such as a plant canopy, are computed without resolving the air/solid boundaries, the dependent variables must be regarded as having been volume averaged, the operation usually being indicated by $\langle\ \rangle$, over a length scale ℓ_a much larger than the scale of the solid parts. Wang and Takle (1995a) and Lien et al. (2004) have shown that for flows such as the present one, which are inhomogeneous on scales greater than ℓ_a, there is a logical advantage to constructing statistics as the time average of the spatial average, as opposed to the spatial average of the conventional time average that is considered by Raupach and Shaw (1982). The distinction between the two averaging strategies essentially amounts to a point of view, rather than a definitive step toward a rigorous

formulation of a RANS closure; either way, heuristic steps are unavoidable. Nonetheless, in this paper we follow Lien et al. (2004), and regard the dependent variables as being the time average of a local spatial average, because this interpretation clarifies the specification of the sources and sinks of turbulent kinetic energy.

To illustrate the averaging, we may take as an example the normal velocity component $u = u(x, y, z, t)$. The two basic decompositions are

$$u = \overline{u} + u' \quad \text{and} \quad u = \langle u \rangle + u'', \tag{1}$$

where $\overline{u'} = 0$ and $\langle u'' \rangle = 0$. For clarity in understanding the meanings of the terms it is helpful to substitute each of the above definitions into the other, yielding the expressions

$$u = \langle \overline{u} \rangle + \overline{u}'' + u' \quad \text{and} \quad u = \langle \overline{u} \rangle + \langle u' \rangle + u'', \tag{2}$$

where we presuppose that the averaging operations commute, that is, $\overline{\langle u \rangle} \equiv \langle \overline{u} \rangle$; to reconstruct the local instantaneous velocity from the *double* average, two deviations need to be added, their sum being

$$\tilde{u} \equiv \overline{u}'' + u' \equiv \langle u' \rangle + u''. \tag{3}$$

Now, for convenience introducing the notation $U = \overline{\langle u \rangle} = \langle \overline{u} \rangle$, in order to simulate a windbreak flow we need to specify the governing equations for the continuous spatial fields of the mean velocity U_i and other statistics. In this paper we assume the time average is of a sufficient duration that the resulting statistics are time independent (steady-state RANS).

It is well known (Wilson and Shaw 1977; Raupach and Shaw 1982; Finnigan 1985; Miguel et al. 2001; Lien et al. 2004) that as a result of the volume averaging, additional terms arise in the momentum equations and formally account for drag on the solid. The result of locally volume averaging the momentum equation is

$$\frac{\partial \langle u_i \rangle}{\partial t} + \frac{\partial \langle u_j \rangle \langle u_i \rangle}{\partial x_j} = \frac{\partial \langle p \rangle}{\partial x_i} - \frac{\partial \langle u_i'' u_j'' \rangle}{\partial x_j} + \frac{g}{T_0} \langle T \rangle \delta_{3i} + f_i, \tag{4}$$

where viscous momentum transport has been neglected, p and T are the kinematic pressure departure and the temperature departure from a hydrostatic and adiabatic reference state, respectively, and f_i, arising from the volume integration, represents the drag of the solid obstacles on the flow. Now, by introducing the expansion $\langle u_i \rangle = \langle \overline{u}_i \rangle + \langle u_i' \rangle$ and time averaging, the steady-state mean momentum equation is

$$\frac{\partial \langle \overline{u}_j \rangle \langle \overline{u}_i \rangle}{\partial x_j} = \frac{\partial \langle \overline{p} \rangle}{\partial x_i} + \frac{\partial \tau_{ij}}{\partial x_j} + \frac{g}{T_0} \langle \overline{T} \rangle \delta_{3i} + \overline{f}_i. \tag{5}$$

The modeling of the kinematic stress tensor

$$\tau_{ij} = -\overline{\langle u_i' \rangle \langle u_j' \rangle} + \overline{\langle u_i'' u_j'' \rangle} \tag{6}$$

is discussed later in section 2d, but, to anticipate, we shall neglect the poorly understood component[1] $\overline{\langle u_i'' u_j'' \rangle}$ and use the approximation

$$\tau_{ij} \approx -\overline{\langle u_i' \rangle \langle u_j' \rangle}. \tag{7}$$

The normal stresses τ_{xx} (etc.) will usually be denoted by the more familiar $-\sigma_u^2$. In line with all this, and again following Lien et al. (2004), the instantaneous resolved-scale turbulent kinetic energy is *defined* as

$$\kappa = \frac{1}{2} \langle u_i' \rangle \langle u_i' \rangle, \tag{8}$$

and its time average

$$k \equiv \overline{\kappa} = \frac{1}{2} \overline{\langle u_i' \rangle \langle u_i' \rangle} = \frac{1}{2} (\sigma_u^2 + \sigma_v^2 + \sigma_w^2) \tag{9}$$

is the model's turbulent kinetic energy (TKE) variable. Please note the use of "k" here to simplify the notation $\overline{\kappa}$ of Lien et al. Although this is the usual symbol for the TKE in numerical models, it carries a specific definition here.

b. Mean momentum sink

The source term f_i in Eq. (4) formally represents viscous and form drag on the unresolved solid parts. Because we are interested here in a thin, porous fence taken to be perpendicular to the x axis and located at $x = 0$, the drag f_i must contain as a factor the delta function $\delta(x - 0)$, having units (m^{-1}), and localizing the momentum sink on the x axis. Conventionally f_x is modeled as the projection onto the x axis of a force that is proportional to the square of the magnitude of the mean (resolved) velocity.

It is more difficult to parameterize the instantaneous vector drag force on a thin fence, than on an isotropic, extensive distribution of solid parts, such as a plant canopy (or wide, natural shelterbelt). In this paper we shall for simplicity *assume* that, as a first approximation, the instantaneous kinematic pressure drop along the x axis across the fence can be expressed in terms of the volume-averaged normal velocity $\langle u(0, y, z, t) \rangle$ at the fence, namely,

$$p_1 - p_2 = \Delta p(y, z, t) = k_{r0} \langle u \rangle |\langle u \rangle| \tag{10}$$

(independent variables not shown for $\langle u \rangle$). Here, k_{r0} is the resistance coefficient of the windbreak screen material for a stream penetrating at normal incidence, and can be considered to be *defined* by this equation [note that Eq. (10) assumes the pressure drop is not affected by any component of the volume (ℓ_a)-averaged velocity parallel to the fence; the pressure drop $p_1 - p_2$ is not observable, because after the (implicit) local volume averaging it is no longer clear what "across the fence"

[1] Lien et al. (2004) show that the shear stress may equivalently be expressed as $\tau_{ij} = -\langle \overline{u}_i' \overline{u}_j' \rangle - \langle \overline{u}_i'' \overline{u}_j'' \rangle$, where the second term is known as the dispersive momentum flux.

actually means]. This usage is consistent with the definition of a resistance coefficient $k_r(\alpha)$ for arbitrary angle (α) of passage given by Laws and Livesey (1978), a definition that scales the pressure drop on the square of the wind *speed* (not, N.B., the square of the normal component), and in terms of which $k_{r0} \equiv k_r(0)$. Thus, Eq. (10) applies irrespective of the angle of incidence (β) of the mean wind and of the local (computed) angle of passage through the fence [for clarification see Eqs. (1) and (2) of Wilson and Flesch (2003)]. It is best regarded as a plausible estimate of an apparent force on the volume-averaged flow, a force oriented perpendicular to the fence (or almost so) that vanishes away from it.

Components of the local drag force that are *parallel* to the fence cause discontinuities in the corresponding velocity components across the fence (Taylor and Batchelor 1949). They can thus be written

$$f_y(y, z, t) = \langle u(0, y, z, t)\rangle[\langle v(0^-, y, z, t)\rangle - \langle v(0^+, y, z, t)\rangle] \quad \text{and}$$
$$f_z(y, z, t) = \langle u(0, y, z, t)\rangle[\langle w(0^-, y, z, t)\rangle - \langle w(0^+, y, z, t)\rangle], \quad (11)$$

where $\langle v(0^-, y, z, t)\rangle$ and $\langle v(0^+, y, z, t)\rangle$ give the parallel velocity component on (respectively) the upwind and downwind sides of the fence (etc.). Equation (11) equates the parallel drag to the *difference* between the instantaneous (kinematic) momentum flux densities on each side of the fence; the normal velocity $\langle u(0, y, z, t)\rangle$ does change from one side to the other, because air does not disappear within the fence. In Eq. (11) one would like to regard $\langle\ \rangle$ as an area average in the y–z plane, so as not to smear out the upwind/downwind discontinuity. However, even if that unwanted condition on their validity could be accepted, from the perspective of a numerical model these estimates of parallel drag are anyway problematic, because the finite grid length Δx of computations will not permit to discriminate the transverse velocities at $x = (0^-, 0^+)$. Alternative expressions of Eq. (11) in terms of the entry and exit orientations of the wind vector offer no advantage in this respect. Thus, for simplicity, and because (unless the wind blows parallel to the fence) it must be far smaller than the normal component, the parallel component of the drag will be neglected, and the instantaneous effect of the fence on the flow will be expressed

$$f_x = -k_{r0}\langle u\rangle|\langle u\rangle|\delta(x - 0)s(z - h),$$
$$f_y = 0, \quad \text{and} \quad f_z = 0, \quad (12)$$

where $s(z - h)$ is a dimensionless unit step function localizing the drag to $z/h \leq 1$. If we substitute $\langle u\rangle = \langle\overline{u}\rangle + \langle u'\rangle$, perform a truncated binomial expansion on $|\langle u\rangle| = \sqrt{\langle u\rangle^2}$, then time average, we obtain

$$\overline{f}_x = -k_{r0}(\langle\overline{u}\rangle^2 + \overline{\langle u'\rangle^2})\delta(x - 0)s(z - h), \quad (13)$$

(while $\overline{f}_y = \overline{f}_z = 0$) or in the shorthand notation

$$\overline{f}_x = -k_{r0}(U^2 + \sigma_u^2)\delta(x - 0)s(z - h). \quad (14)$$

This is the same as the momentum sink used by W85 (p. 135), who found the term in the variance $\sigma_u^2 = \overline{\langle u'\rangle^2}$ to be unimportant (for the case $h/z_0 = 600$; it could be more important for smaller h/z_0). It bears repetition that the numerical value of k_{r0} is a property of the plastic screen, and that in simulations one does not adjust its value according to the prescribed approach wind direction (β) or the (computed) local wind direction at the fence, arctan (V/U). Again, this stems from the assumption that it is the *normal* component of the wind that controls the pressure loss across the fence.

There is one necessary change to Eq. (14) that is potentially important for the ''practical numerics'' of solving the model equations; note that this momentum sink is insensitive to the sign of the mean velocity U, an obvious flaw (the drag must oppose the flow). This is a consequence of the approximation of small fluctuations that is implicit in the binomial expansion, and needs to be fixed: one simply substitutes $U|U|$ for U^2 in Eq. (14). This ensures a realistic feedback (i.e., drag in the right direction) on large velocities, that may transiently develop while iterating to a solution.

Wilson and Flesch (2003) gave momentum sinks in the U and V momentum equations in a frame of reference whose x axis, unlike here, was aligned with the mean wind direction far upwind from the fence. When the equations given by Wilson and Flesch are rotated into the present frame of reference, Eq. (14) results for $\overline{f}_x$, and as expected $\overline{f}_y = 0$.

c. Modeled mean momentum equations

The model mean momentum equations, expressed in the shorthand notation, are

$$\frac{\partial}{\partial x}(U^2 + \sigma_u^2 + P) + \frac{\partial}{\partial z}(UW - \tau_{xz}) = -k_{r0}(U|U| + \sigma_u^2)\delta(x - 0)s(z - h),$$
$$\frac{\partial}{\partial x}(UV - \tau_{xy}) + \frac{\partial}{\partial z}(VW - \tau_{yz}) = 0, \quad \text{and}$$
$$\frac{\partial}{\partial x}(UW - \tau_{xz}) + \frac{\partial}{\partial z}(W^2 + \sigma_w^2 + P) = \frac{g}{T_0}T, \quad (15)$$

where P is the local disturbance in mean kinematic pressure caused by interaction of the wind with obstacles, and T (with a slight inconsistency in notation relative to its earlier appearance) is now the mean temperature deviation from a hydrostatic adiabatic reference state (of course, these equations are valid in the Boussinesq approximation). Because of the assumption $\partial/\partial y = 0$, the momentum equations do not involve the along-fence variance σ_v^2, but all other components of the stress tensor play a role, in principle, and their specification requires that a turbulence closure be invoked.

d. The Reynolds stress equation

If we may neglect the component $\langle \overline{u_i'' u_j''} \rangle$ of the compound Reynolds stress that emerges from the joint time–volume averaging, the momentum equations can be closed by making approximations in the Reynolds equation, that is, the budget equation for $-\tau_{ij} = \overline{\langle u_i' \rangle \langle u_j' \rangle}$. This latter is derivable in the usual manner by operations with the instantaneous, locally volume-averaged momentum Eq. (4), and in its form, it differs from the standard $\overline{u_i' u_j'}$ equation only in the presence of a term arising from the momentum sink. Thus, assuming steady state and making the usual assumption with respect to the viscous terms at high Reynolds number, the stress budget can be written (Lumley and Khajeh-Nouri 1974)

$$\begin{aligned}
&\frac{\partial}{\partial x_k}(U_k \overline{\langle u_i' \rangle \langle u_j' \rangle}) \\
&\quad = -\overline{\langle u_i' \rangle \langle u_k' \rangle} \frac{\partial U_j}{\partial x_k} - \overline{\langle u_j' \rangle \langle u_k' \rangle} \frac{\partial U_i}{\partial x_k} \\
&\qquad - \frac{\partial}{\partial x_k} \overline{\langle u_k' \rangle \langle u_i' \rangle \langle u_j' \rangle} - \overline{\langle u_j' \rangle \frac{\partial \langle p' \rangle}{\partial x_i} + \langle u_i' \rangle \frac{\partial \langle p' \rangle}{\partial x_j}} \\
&\qquad + \frac{g}{T_0} (\overline{\langle u_i' \rangle \langle T' \rangle} \delta_{i3} + \overline{\langle u_j' \rangle \langle T' \rangle} \delta_{j3}) - \frac{2}{3} \epsilon \delta_{ij} + \epsilon_{ij},
\end{aligned} \tag{16}$$

where

$$\epsilon_{ij} = \overline{\langle u_j' \rangle f_i' + \langle u_i' \rangle f_j'} \tag{17}$$

arises from the drag on the solid obstacles and is not to be confused with the ordinary viscous dissipation ϵ. It is usual as a precursor to formulating closure approximations that the pressure term be expanded

$$\begin{aligned}
\Pi_{ij} &= \overline{\langle u_j' \rangle \frac{\partial \langle p' \rangle}{\partial x_i} + \langle u_i' \rangle \frac{\partial \langle p' \rangle}{\partial x_j}} \\
&= \frac{\partial}{\partial x_i} \overline{\langle p' \rangle \langle u_j' \rangle} + \frac{\partial}{\partial x_j} \overline{\langle p' \rangle \langle u_i' \rangle} - \overline{\langle p' \rangle \left(\frac{\partial \langle u_i' \rangle}{\partial x_j} + \frac{\partial \langle u_j' \rangle}{\partial x_i} \right)} \\
&= P_{ij}^T - R_{ij}.
\end{aligned} \tag{18}$$

The first two terms, whose sum has been labeled P_{ij}^T, represent ''pressure transport.'' The final term is called the ''pressure strain'' or ''pressure rate of strain'' because it involves the fluctuating velocity gradient tensor. This (R_{ij}) is also known as the ''redistribution term'' because (in incompressible, i.e., nondivergent, flows) it vanishes upon contraction ($i = j$) and so does not affect the total TKE, while it acts to equalize the partitioning of TKE into its components.

For the present flow about a long, porous planar barrier, there is (by assumption) only a single nonzero component of the drag fluctuation f_i',

$$\begin{aligned}
f_x' = &-k_{r0} \delta(x - 0) s(z - h) \\
&\times (\langle u' \rangle \langle u' \rangle + 2 \langle \overline{u} \rangle \langle u' \rangle - \overline{\langle u' \rangle \langle u' \rangle}),
\end{aligned} \tag{19}$$

in contrast with the formulation of Lien et al. (2004), which parameterizes the drag on a three-dimensional array of cuboid buildings. Consequently it follows from Eq. (17) that

$$\begin{aligned}
\epsilon_{xx} &= -k_{r0} \delta(x - 0) s(z - h) (4U\sigma_u^2 + 2\overline{\langle u' \rangle \langle u' \rangle \langle u' \rangle}), \\
\epsilon_{yy} &= \epsilon_{zz} = \epsilon_{yz} = 0, \\
\epsilon_{xz} &= -k_{r0} \delta(x - 0) s(z - h) (2U\overline{\langle u' \rangle \langle w' \rangle} + \overline{\langle w' \rangle \langle u' \rangle \langle u' \rangle}), \\
\text{and} \\
\epsilon_{xy} &= -k_{r0} \delta(x - 0) s(z - h) (2U\overline{\langle u' \rangle \langle v' \rangle} + \overline{\langle v' \rangle \langle u' \rangle \langle u' \rangle}),
\end{aligned} \tag{20}$$

in which the triple correlation terms, which (incidentally) *could* permit the *gain* of resolved-scale kinetic energy from the subfilter scales, have not been retained in the numerical models (from here on we shall usually suppress the $\langle\ \rangle$, to simplify the notation). It is interesting to note the absence of wake-conversion sinks in the conservation equations for the variances σ_v^2, σ_w^2 of the velocity components *parallel* to the fence. Of course this follows from the assumptions [Eq. (12)] of the form of the momentum sinks, but to the extent that those assumptions are valid, the occurrence of a sink for σ_u^2 where there is none for σ_v^2 [Eq. (20)] may in part explain the observation (Part I, their Fig. 16) that in the leeward ''quiet zone'' the variance σ_u^2 of the normal component is reduced by a greater fraction and over a longer leeward distance, than is the variance σ_v^2 of the parallel component.

Lien et al. have stressed the absence in the $\overline{\kappa}$ equation (time-averaged resolved-scale kinetic energy) of any source term representing gain of turbulent kinetic energy from the mean kinetic energy $(1/2)\langle \overline{u}_i \rangle \langle \overline{u}_i \rangle$, and noted the similarity in this regard of their more rigorous formulation with Wilson's (1988) heuristic spectral division into large-scale kinetic energy (SKE) and wake-scale kinetic energy (WKE), a separation that was justified by a presupposition that wake eddies must necessarily be of such a (small) scale as to lie outside the SKE spectrum.

e. Rao–Wyngaard–Coté second-order closure

Rao, Wyngaard, and Coté (hereinafter RWC) introduced their closure in the context of modeling local advection (Rao et al. 1974a,b; Bink 1996; Wilson et al. 2001). RWC is not very different from other common second-order closures, and in particular it differs essentially from the simplest of the closures of Launder et al. (1975, hereinafter LRR) only in that it does not parameterize the ''rapid'' part of the pressure strain (there are also habitually some differences in the specification of closure coefficients, compensating the differences in the equation sets in the sense that they optimally tune the different closures to the same reference flow).

Rather than start from the decomposition given by

Eq. (18), RWC instead rearranged the stress budget equation by regrouping the turbulent transport and pressure terms

$$\frac{\partial}{\partial x_k}\overline{u_i' u_j' u_k'} + \overline{u_i' \frac{\partial p'}{\partial x_j} + u_j' \frac{\partial p'}{\partial x_i}} = \frac{\partial}{\partial x_k}\overline{\left(u_i' u_j' + \frac{2}{3}p'\delta_{ij}\right)u_k'} + \left(\overline{u_i' \frac{\partial p'}{\partial x_j} + u_j' \frac{\partial p'}{\partial x_i}} - \frac{2}{3}\frac{\partial \overline{p' u_k'}}{\partial x_k}\delta_{ij}\right) = \tilde{T}_{ij} - \tilde{R}_{ij}. \quad (21)$$

RWC modeled the transport term $\tilde{T}_{ij}$ by assuming

$$\overline{\left(u_i' u_j' + \frac{2}{3}p'\delta_{ij}\right)u_k'} = -a_t \tau \overline{u_k' u_m'}\frac{\partial \overline{u_i' u_j'}}{\partial x_m}, \quad (22)$$

where a_t is a dimensionless coefficient and $\tau = 2k/\epsilon$ is a constructed turbulence time scale. They modeled the second term $\tilde{R}_{ij}$ as an isotropizing redistribution term,

$$\overline{u_i' \frac{\partial p'}{\partial x_j} + u_j' \frac{\partial p'}{\partial x_i}} - \frac{2}{3}\frac{\partial \overline{p' u_k'}}{\partial x_k}\delta_{ij} = \frac{c_{ij}}{\tau}\left(\overline{u_i' u_j'} - \frac{2}{3}k\delta_{ij}\right), \quad (23)$$

where k is the TKE and the c_{ij} are dimensionless coefficients. All second-order closures include a term similar to this one, attributed to Rotta, and considered to parameterize the ''turbulence–turbulence'' terms in the equation for the pressure strain (LRR; Launder 1989).

With these closure assumptions, the RWC model equation for σ_u^2 is

$$\frac{\partial}{\partial x}\left(U\sigma_u^2 - a_t \tau \sigma_u^2 \frac{\partial \sigma_u^2}{\partial x}\right) + \frac{\partial}{\partial z}\left(W\sigma_u^2 - a_t \tau \sigma_w^2 \frac{\partial \sigma_u^2}{\partial z}\right) = -2\sigma_u^2 \frac{\partial U}{\partial x} + 2\tau_{xz}\frac{\partial U}{\partial z} - \frac{c_{11}}{\tau}\left(\sigma_u^2 - \frac{2}{3}k\right) - \frac{\partial}{\partial x}\left(a_t \tau \tau_{xz}\frac{\partial \sigma_u^2}{\partial z}\right) - \frac{\partial}{\partial z}\left(a_t \tau \tau_{xz}\frac{\partial \sigma_u^2}{\partial x}\right) - \frac{2}{3}\epsilon + \epsilon_{xx}, \quad (24)$$

where ϵ_{xx} is the previously given source term (a TKE sink) due to interaction of the flow with the fence, and equations for the other variance components are analogous.

The RWC τ_{xz} equation is

$$\frac{\partial}{\partial x}\left(U\tau_{xz} - a_t \tau \sigma_u^2 \frac{\partial \tau_{xz}}{\partial x}\right) + \frac{\partial}{\partial z}\left(W\tau_{xz} - a_t \tau \sigma_w^2 \frac{\partial \tau_{xz}}{\partial z}\right) = -\tau_{xz}\frac{\partial U}{\partial x} + \sigma_w^2 \frac{\partial U}{\partial z} + \sigma_u^2 \frac{\partial W}{\partial x} - \tau_{xz}\frac{\partial W}{\partial z} + \frac{g}{T_0}(\overline{u'\theta'} + 0.61 T_0 \overline{u'q'}) - \frac{c_{13}}{\tau}\tau_{xz} - \frac{\partial}{\partial x}\left(a_t \tau \tau_{xz}\frac{\partial \tau_{xz}}{\partial z}\right) - \frac{\partial}{\partial z}\left(a_t \tau \tau_{xz}\frac{\partial \tau_{xz}}{\partial x}\right) - \epsilon_{xz}. \quad (25)$$

Note that because $\tau_{xz} = -\overline{\langle u'\rangle\langle w'\rangle}$, the earlier-defined ϵ_{xz} is subtracted on the rhs of the τ_{xz} equation, where it had been added on the rhs of the $\overline{\langle u'\rangle\langle w'\rangle}$ equation.

Last, the RWC ϵ equation is

$$\frac{\partial}{\partial x}\left(U\epsilon - a_{t\epsilon}\tau\sigma_u^2\frac{\partial \epsilon}{\partial x}\right) + \frac{\partial}{\partial z}\left(W\epsilon - a_{t\epsilon}\tau\sigma_w^2\frac{\partial \epsilon}{\partial z}\right) = \frac{\epsilon}{k}[C_{\epsilon_1}(P - \epsilon_{fd}) - C_{\epsilon_2}\epsilon] - \frac{\partial}{\partial x}\left(a_{t\epsilon}\tau\tau_{xz}\frac{\partial \epsilon}{\partial z}\right) - \frac{\partial}{\partial z}\left(a_{t\epsilon}\tau\tau_{xz}\frac{\partial \epsilon}{\partial x}\right), \quad (26)$$

where

$$P_{uu} = -2\sigma_u^2\frac{\partial U}{\partial x} + 2\tau_{xz}\frac{\partial U}{\partial z}, \quad P_{vv} = 2\tau_{xy}\frac{\partial V}{\partial x} + 2\tau_{yz}\frac{\partial V}{\partial z},$$

$$P_{ww} = 2\tau_{xz}\frac{\partial W}{\partial x} - 2\sigma_w^2\frac{\partial W}{\partial z} + 2\frac{g}{T_0}(\overline{w'T'} + 0.61 T_0 \overline{w'q'}),$$

and

$$P = \frac{1}{2}(P_{uu} + P_{vv} + P_{ww}) \quad (27)$$

are the production rates of variance and TKE (q' is the fluctuation in specific humidity). The heuristic term $\epsilon_{fd} = \epsilon_{xx}/2$ locally reduces the rate of ϵ production in relation to the amount by which TKE production at the fence is offset by wake conversion, and was suggested by Lien et al. (2004); a similar idea was proposed by Green et al. (1992, 1994). Its effect, for the case of a thin windbreak, is minor. To reduce finite-difference errors, it is advantageous to transform Eq. (26) into an equation for the product ($z\epsilon$), which is independent of height in the reference state defined below.

Of course for simulations of the stratified surface layer, the RWC closure entails many more equations, for example, the heat flux budget equations $\overline{u'T'}$ and $\overline{w'T'}$, but these are closed using similar principles and need not be reviewed; for details, see Wilson et al. (2001) and other work cited there.

f. Specification of the RWC closure constants

Like others exploring second-order closures shortly after the Kansas experiments, Rao et al. (1974a,b) presupposed that the von Kármán constant $k_v = 0.35$. Later analyses (e.g., Dyer and Bradley 1982) have supported $k_v = 0.4$, with equality of the eddy diffusivities for momentum, heat, and water vapor in the neutral limit. The point is that if one were to insist on following *exactly* the RWC specification of coefficients—and this comment applies equally to replication of the Mellor (1973) and the Lewellen and Teske (1973) studies—one

would thereby commit to a formulation that is inconsistent with that adopted by most workers now in analysis of measurements, and in particular, with the analysis of the experiment of Part I. The approach taken here is to set $k_v = 0.4$, but otherwise follow the same *logic* as the original proponents of a closure: some constants are specified to tailor the modeled values of observed (normalized) statistics to experimental values (e.g., the values of $\sigma_{u,v,w}/u_*$ in the neutral limit); some few are ''free'' (e.g., in the RWC closure, the coefficient a_t multiplying the transport terms, as well as the coefficients $c_{\epsilon 1}$, $c_{\epsilon 2}$ of the ϵ equation, set by RWC as, respectively, $c_{\epsilon 1} = 1$, $c_{\epsilon 2} = 2$); and others (c_{ij}, c_ϵ) are constrained (as outlined below) by equations that require consistency of the closure with a ''reference flow,'' here chosen to be the neutrally stratified and horizontally homogeneous constant stress (i.e., surface) layer, in the state of local equilibrium (abbreviated ''hh-NSL-le'').

Following Rao et al. (1974a,b), without exception the simulations using their closure used $a_t = 0.15$; however, in some calculations (where noted) the coefficients of the ϵ equation were varied from $c_{\epsilon 1} = 1$, $c_{\epsilon 2} = 2$. The only other variation from the standard specification of parameters usual with RWC was made to ensure that the universal Monin–Obukhov function for heat should have the limit $\phi_H(z/L) \to 1$ as $|z/L| \to 0$ so that in this neutral limit the turbulent Prandtl should be unity.

g. The reference flow

Let (u_0, v_0, w_0) be the velocity vector in a frame $F_0(x_0, y_0)$ aligned with the mean wind vector, and let (u, v, w) be the velocity for an arbitrary orientation of the coordinate system at angle β away from the x_0 axis. Velocities in the two frames are related by the transformation

$$u = u_0 \cos\beta + v_0 \sin\beta \quad \text{and}$$
$$v = -u_0 \sin\beta + v_0 \cos\beta. \tag{28}$$

In the reference flow we assume the shear stress to be constant, and parallel to the mean wind. Thus, the single nonvanishing component of the kinematic shear stress $\tau_{xz0} = -\overline{u_0' w_0'}$ defines the velocity scale $u_* = \sqrt{-\overline{u_0' w_0'}}$. The reference flow is then defined as

$$U_0(z) = \frac{u_*}{k_v} \ln\left(\frac{z}{z_0}\right), \qquad V_0 = W_0 = 0,$$
$$\overline{u_0' w_0'} = -u_*^2, \qquad \overline{v_0' w_0'} = \overline{u_0' v_0'} = 0,$$
$$\overline{u_0'^2} = c_{uu0} u_*^2, \qquad \overline{v_0'^2} = c_{vv0} u_*^2, \qquad \overline{w_0'^2} = c_{ww0} u_*^2,$$
$$k = \frac{1}{2}(c_{uu0} + c_{vv0} + c_{ww0}) u_*^2, \quad \text{and} \quad \epsilon(z) = \frac{u_*^3}{k_v z}, \tag{29}$$

where quantities that vary with height in the ideal neutral surface layer (hh-NSL-le) are so designated (all others are height independent), and (to repeat, in the present work) $k_v = 0.4$. The normalized variances c_{uu0} (etc.) are not to be confused with the coefficients c_{ij} introduced in Eq. (23).

h. Definition of the reference flow in the arbitrary coordinate system

Projecting the shear stress vector (recall assumed, in so far as the reference flow is concerned, to be aligned with the x_0 axis) onto the arbitrary coordinate system we have

$$\tau_{xz} = -u_{*u}^2 = -u_*^2 \cos\beta,$$
$$\tau_{yz} = -u_{*v}^2 = -u_*^2 \sin\beta, \quad \text{and}$$
$$\tau_{xy} = 0, \tag{30}$$

where u_{*u}, u_{*v} are introduced for convenience, and evidently $u_*^4 = u_{*u}^4 + u_{*v}^4$. Similarly the components of the mean wind are

$$U(z) = \frac{u_* \cos\beta}{k_v} \ln\left(\frac{z}{z_0}\right),$$
$$V(z) = \frac{u_* \sin\beta}{k_v} \ln\left(\frac{z}{z_0}\right), \quad \text{and}$$
$$W = 0. \tag{31}$$

It is important here to emphasize that $u_* \cos\beta \neq u_{*u}$ and that $u_* \sin\beta \neq u_{*v}$, that is, that a prescription $\partial U/\partial z = u_{*u}/(k_v z)$ would be incompatible with the definition of u_{*u}. The relationships given above uphold the requirement that in the reference flow the production rate P and dissipation rate ϵ of TKE balance, that is,

$$\epsilon = P = \tau_{xz}\frac{\partial U}{\partial z} + \tau_{yz}\frac{\partial V}{\partial z} = \frac{u_*^3}{k_v z}. \tag{32}$$

Last, as the orientation of the coordinate system is arbitrary, so too are the relative values of the normalized variances c_{uu}, c_{vv}. However, one has definite ideas of the respective values for $\sigma_u^2 = c_{uu0} u_*^2$ and $\sigma_v^2 = c_{vv0} u_*^2$ in the case that the x axis is parallel with the mean wind, that is, $V = 0$; typically we may expect (in the neutral limit, and only very approximately) $c_{uu0} \sim 4$, $c_{vv0} \sim 2$, reflecting the fact that shear production feeds the streamwise but not the transverse variance. From Eqs. (28), the normalized variances for the arbitrary coordinate orientation are

$$c_{uu} = c_{uu0} \cos^2\beta + c_{vv0} \sin^2\beta \quad \text{and}$$
$$c_{vv} = c_{uu0} \sin^2\beta + c_{vv0} \cos^2\beta. \tag{33}$$

Thus, in the arbitrary coordinate system the reference state is defined by Eqs. (31)–(33), and

$$\sigma_u^2 = c_{uu} u_*^2, \qquad \sigma_v^2 = c_{vv} u_*^2, \qquad \sigma_w^2 = c_{ww} u_*^2,$$

$$k = \frac{1}{2}(c_{uu} + c_{vv} + c_{ww})u_*^2$$

$$\equiv \frac{1}{2}(c_{uu0} + c_{vv0} + c_{ww0})u_*^2, \quad \text{and} \quad \epsilon(z) = \frac{u_*^3}{k_v z}. \quad (34)$$

The RWC closure, like other second-order turbulence closures, introduces a turbulence time scale (τ) computed from the numerical values of k and ϵ,

$$\tau = \frac{2k}{\epsilon} \underset{\text{(ref)}}{\rightarrow} \frac{k_v z}{u_*}\frac{2k}{u_*^2}, \quad (35)$$

where the limit $\rightarrow_{\text{(ref)}}$ denotes ''in the reference state.''

i. Requiring the 1D equations to reproduce the reference state

The coefficients entering into the governing equations must be chosen so that the structure defined by Eqs. (31)–(35) is embedded, in order that equilibrium simulations will generate exactly that state.

Beginning with the shear stress equations, and recalling that in the reference state (by requirement) the shear stress is height independent, the budget for τ_{xz} reduces to

$$0 = \overline{w'^2}\frac{\partial U}{\partial z} - c_{13}\frac{\tau_{xz}}{\tau}. \quad (36)$$

Upon substituting for τ and writing $\sigma_w^2 = c_{ww}u_*^2$, $\tau_{xz} = u_*^2 \cos\beta$, simplification yields

$$c_{13} = c_{ww}\frac{2k}{u_*^2}, \quad (37)$$

while the complete symmetry between u and v in the arbitrary coordinate system implies $c_{23} \equiv c_{13}$ (the coefficient c_{12} was given the same value). Similarly, in the reference state the budget for σ_u^2 reduces to

$$0 = \tau_{xz}\frac{\partial U}{\partial z} - \frac{2}{3}\epsilon - c_{11}\frac{\sigma_u^2 - (2/3)k}{\tau}, \quad (38)$$

and substitutions result in

$$c_{11} = \frac{n(6\cos^2\beta - 2)}{3c_{uu} - n}, \quad (39)$$

where $n = 2k/u_*^2$. The analogous balance for σ_v^2 results in

$$c_{22} = \frac{n(6\sin^2\beta - 2)}{3c_{vv} - n}, \quad (40)$$

while for σ_w^2, which is not sensitive to choice of the coordinate orientation, the desired balance is assured provided

$$c_{33} = \frac{2n}{n - 3c_{ww}}. \quad (41)$$

Last, in the reference state, the ϵ equation reduces to

$$\frac{\partial}{\partial z}\left(-a_{t\epsilon}\tau\sigma_w^2\frac{\partial \epsilon}{\partial z}\right) = \frac{\epsilon}{k}(c_{\epsilon 1}P - c_{\epsilon 2}\epsilon), \quad (42)$$

with $P = \epsilon$ (note that unlike in all the other equilibrium equations, in this case the diffusion term does not vanish in the reference state). Substitutions result in the requirement that

$$a_{t\epsilon} = \frac{2(c_{\epsilon 2} - c_{\epsilon 1})}{k_v^2 c_{ww} n^2}. \quad (43)$$

Please note that the equations determining c_{11}, c_{12}, c_{33}, c_{13}, . . . must be provided with one's specifications for observable statistics (like σ_w^2/u_*^2) but do not depend on one's choice for k_v. On the other hand the transport coefficient $a_{t\epsilon}$ (playing the role of c_ϵ in the usual jargon of the ϵ equation, with $c_\epsilon = 2a_{t\epsilon}$) is constrained by Eq. (43) to depend on k_v (and the ''free'' coefficients $c_{\epsilon 1}$, $c_{\epsilon 2}$, as well as the observables σ_w/u_*, k/u_*^2), while owing to the fact that in the reference state the balance equations for the components of the stress tensor are local (i.e., diffusion terms vanish), the other transport coefficient a_t is free.

For further details in the specification of coefficients of the RWC closure, please see Wilson et al. (2001), in particular as regards the ''tuning'' of the equations that determine the temperature and humidity flux and variance fields, where a coefficient d_3 takes on a value compatible with the desired value of the turbulent Prandtl number (the present choice being unity) in the reference state.

j. Launder–Reece–Rodi closure

For the neutral, perpendicular case only, the shelter observations and the computations using the RWC closure will be compared with alternative computations from the more widely used second-order closure of LRR. As far as equations, numerical method, and closure constants are concerned, the present simulations using LRR follow W85 exactly. In particular, they use LRR's simplified model of the pressure strain

$$R_{ij} = \overline{p'\left(\frac{\partial u_i'}{\partial x_j} + \frac{\partial u_j'}{\partial x_i}\right)}$$

$$= -c_1\frac{\epsilon}{k}\left(\overline{u_i'u_j'} - \frac{2}{3}k\delta_{ij}\right) - c_2\left(P_{ij} - \frac{2}{3}P\delta_{ij}\right), \quad (44)$$

where the second term is known as ''isotropization of production'' (LRR), and the production rates are given by Eq. (27). The sum of turbulent and pressure transport terms was modeled as Eq. (22), this being attributed to Daly and Harlow (1970). According to Launder (1989) ''The role of pressure fluctuations in modifying the level of the second moments is arguably the liveliest debating point in second-moment closures'' whereas outside the near-wall sublayer where viscosity is important ''few of

the important anomalies one finds in predictions of inhomogeneous flows can be traced to weakness in the diffusion model,'' that is, in Eq. (22).

In order to connect with the usual notation for the LRR model please note that RWC's coefficient a_t and LRR's c_s' are connected by $c_s' = 2a_t$, and so there is a small numerical difference in the treatment of the transport term in that the present LRR simulations follow LRR and set $c_s' = 0.25$ (except in a single comparative case noted in Fig. 6), while the RWC simulations follow RWC and set $a_t = 0.15$. The LRR ϵ equation is identical to that of RWC, with only a notational difference ($c_\epsilon = 2a_{t\epsilon}$ connects the LRR terminology on the left with the RWC terminology on the right). Irrespective of the terminology, c_ϵ (or $a_{t\epsilon}$) is determined from the other coefficients ($c_{\epsilon 1}$, $c_{\epsilon 2}$, and chosen values for the equilibrium variances) by requiring that the set of equations correctly reduce to the equilibrium state. In summary then, the ''tuning'' of the LRR closure coefficients is here identical to that given by W85 (his Table 1), with the same input values of the observables ($\sigma_u^2/u_*^2 = 2.87$, etc.).

k. Details of numerical method

Because due to the symmetry $\partial/\partial y = 0$ the V field is not linked to the mean pressure field, it was not necessary to offset the V grid points on the y axis relative to P grid points; hence, V was collocated with U and the mean scalars.

Users of the semi-implicit method for pressure-linked equations (SIMPLE)-type solution procedure may have had the experience that, having functioned very satisfactorily for a certain grid, the algorithm may incomprehensibly fail to converge when one alters Δx or Δz or the grid aspect ratio $\Delta z/\Delta x$; that is, on any given grid, convergence is not assured a priori. More important, repeatability of any simulation hinges on precise replication of the grid (except if grid independence is attained, and it has not been here), so that it is not pedantic to provide full details. A staggered grid identical to that defined by W85 was used, its inflow and outflow boundaries chosen to run through U ($=V$) grid points, while the ground and the upper boundary ran through W grid points. The scalars (mean potential temperature T and mean humidity Q) were collocated with U (and V), while all second-order quantities were placed at the intersection of the vertical planes of U grid points with the horizontal planes of W grid points. Vertical W planes lay equidistant from vertical U planes, so that (unless grid size Δx = constant) U grid points were not x-wise central in their control volumes. On the other hand, horizontal U planes were centered between the horizontal W planes. Details of domain size and grid length will be given for each simulation.

l. Boundary conditions

For the RWC simulations inflow profiles of the velocity statistics were specified as the 1D (i.e., equilibrium) solution, for prescribed approach flow state and orientation (u_{*0}, L, z_0, β), while for the LRR closure (neutral, perpendicular case only) ideal analytical profiles were imposed[2] (semilogarithmic mean wind profile, constant shear stress, constant velocity variances). In all reported simulations, it was assumed that all properties satisfy $\partial/\partial x = 0$ at the downwind boundary; exploratory computations with enforced recovery to the equilibrium state indicated that this made negligible difference, and in particular was not a cure all for a deficient model.

At the upper boundary ($z = Z_T$), mean vertical velocity $W = 0$ and the fluxes of U and V momentum τ_{xz} and τ_{yz} were held constant at their equilibrium values, driving the modeled flow. Velocity variances along Z_T were directly specified as $\sigma_u^2 = c_{uu}u_{*0}^2$ (etc.).

As is customary, it was assumed that a shallow equilibrium wall layer exists at the lower boundary. Thus, the necessary surface U and V momentum fluxes were computed from the mean velocities U_P and V_P at the lowest velocity grid point (height z_P), according to

$$u_{*\ell} = \frac{k_v\sqrt{U_P^2 + V_P^2}}{\ln(z_P/z_0)}, \qquad \beta_\ell = \arctan\left(\frac{V_P}{U_P}\right),$$

$$\tau_{xz\ell} = -u_{*\ell}^2\cos\beta_\ell, \quad \text{and} \quad \tau_{yz\ell} = -u_{*\ell}^2\sin\beta_\ell, \qquad (45)$$

where ℓ denotes a local surface value. Similarly the needed surface values for other turbulence properties were taken as

$$\sigma_{u\ell}^2 = c_{uu}u_{*\ell}^2, \qquad \sigma_{v\ell}^2 = c_{vv}u_{*\ell}^2,$$

$$\sigma_{w\ell}^2 = c_{ww}u_{*\ell}^2, \quad \text{and} \quad (z\epsilon)_\ell = \frac{u_{*\ell}^3}{k_v}. \qquad (46)$$

In all simulations it was assumed $\tau_{xy} = 0$ along $z = (z_0, Z_T)$. Boundary conditions for thermodynamic variables followed the same principles outlined above (for details see Wilson et al. 2001).

m. Other details

Patankar's power-law interpolation scheme was used to estimate the coefficients linking neighboring grid-point values. As in W85 a simulation was considered to have converged if the computed net momentum flux across the boundaries into the computational domain balanced the drag on the fence, to within 1% or better.

As outlined in Part I [his Eq. (11)] under the assumption that velocity fluctuations are small relative to

[2] When analytic inflow profiles are used in lieu of an appropriate 1D numerical solution, there is a danger of incompatibility of the inflow with the finite-differencing scheme, leading to a possible component in the modeled flow disturbance that is driven by that incompatibility. As detailed by W85, no such problem arose with the LRR scheme.

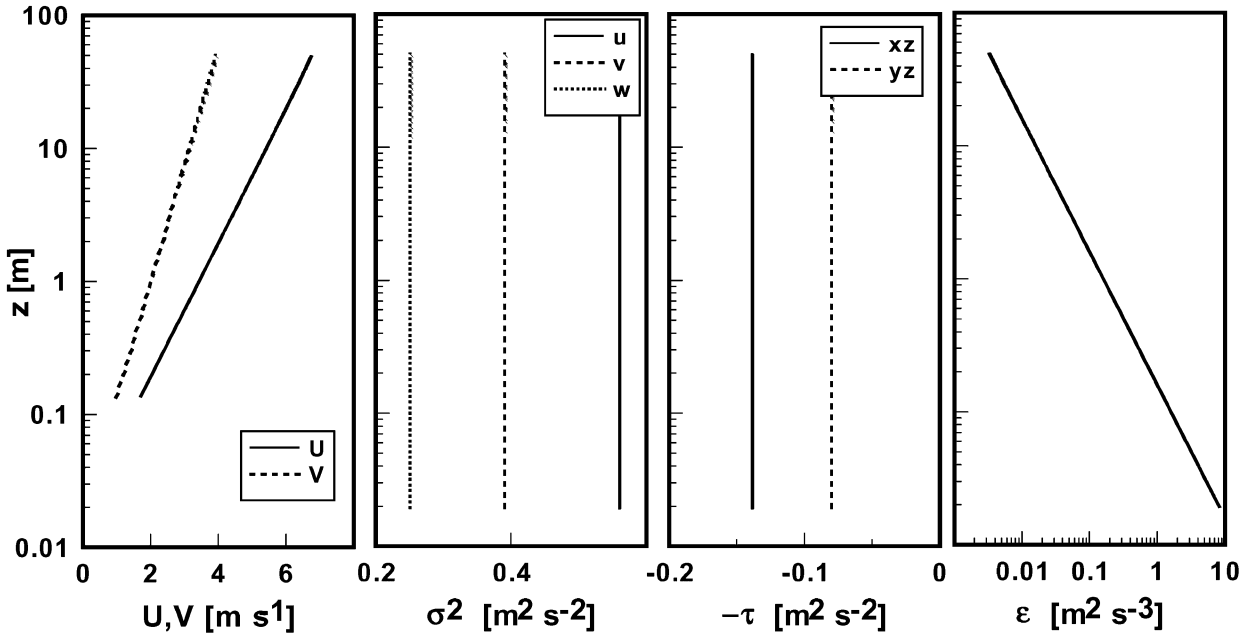

FIG. 3. Equilibrium profiles of velocity statistics from the numerical model with RWC closure, for the neutral case ($u_* = 0.4$ m s^{-1}, $z_0 = 0.019$ m) with $\beta = 30°$.

the magnitude of the mean velocity, mean cup wind speed can be approximately related to the mean velocity components and standard deviations as

$$S \cong Q\left(1 + \frac{\overline{u'^2} + \overline{v'^2}}{2Q^2}\right), \tag{47}$$

where $Q^2 = \overline{u}^2 + \overline{v}^2$. This formula is liable to be inaccurate, however, in the very circumstances in which the distinction between S and Q could be important. Therefore, unless otherwise stated, in the simulations to follow the term in the velocity variances has been neglected, so that (the model's) cup wind speed has been approximated as $S = Q = \sqrt{\overline{u}^2 + \overline{v}^2}$, which has the advantage that if the variances are poorly computed, they will not adversely affect the model's estimate of the cup wind speed.

The second component $-k_{r0}\sigma_u^2$ of the drag term [Eq. (14)] in the U momentum equation has not been included in simulations to be shown; its computed effect was small enough (less than 5%) to warrant that it be omitted, because the accuracy of (computed) σ_u^2 at the fence is in any case doubtful.

3. Computed equilibrium flows

a. Neutral approach flow

Rao et al. (1974a,b) prescribed $k_v = 0.35$, $\sigma_u/u_* = 2$, $\sigma_v/u_* = \sigma_w/u_* = \sqrt{1.75} = 1.32$, $c_{\epsilon 1} = 1$, and $c_{\epsilon 2} = 2$. With these inputs the present RWC code reproduces exactly their $c_{11} = c_{22} = c_{33} = 6.7$, $c_{13} = 13.2$, and $a_{t\epsilon} = 0.165$. However, for reasons given earlier, for the present simulations we assume $k_v = 0.4$. And once having decided to depart from the original coefficients, it seemed appropriate to specify the equilibrium variances in the ranking they are usually reported, namely, $\sigma_u^2 > \sigma_v^2 > \sigma_w^2$ (as seen in a frame aligned with the mean wind). Therefore, the present simulations using the RWC closure used $c_{uu0} = 4$, $c_{vv0} = 1.93$, and $c_{ww0} = 1.56$, corresponding to $\sigma_{u,v,w}/u_* = (2, 1.4, 1.25)$ and $k/u_*^2 = 3.75$. The main virtue of this arbitrary choice is that it follows Bink (1996), in his comprehensive and critical comparison of the RWC model with observations of dry to moist land flow. Other input constants were the equilibrium values for the ratios

$$\frac{\overline{u'T'}}{u_*T_*} = 4 \quad \text{and} \quad \frac{\overline{T'^2}}{u_*T_*} = 5.29, \tag{48}$$

where $T_* = -Q_H/(\rho c_p u_*)$ is the Monin–Obukhov scale for the temperature fluctuations, derived from the kinematic surface heat flux density $Q_H = \rho c_p \overline{w'T'}$. In all simulations the surface resistance to evaporation was specified as infinite (dry system), and so the equations involving humidity play no role.

Figure 3 shows the computed equilibrium velocity statistics for the neutral condition, $u_* = 0.4$ m s^{-1}, $z_0 = 0.019$ m, and $\beta = 30°$. This (reference flow) is the approach flow for neutral RWC simulations of the Ellerslie windbreak observations at 30° obliquity. Note the semilogarithmic profiles of the mean wind components, the height-independent shear stress components, and the $\epsilon \propto z^{-1}$ profile of dissipation rate. This last feature, assured by working with an equation for $z\epsilon$ (rather than ϵ), is the key to the attainment of (length

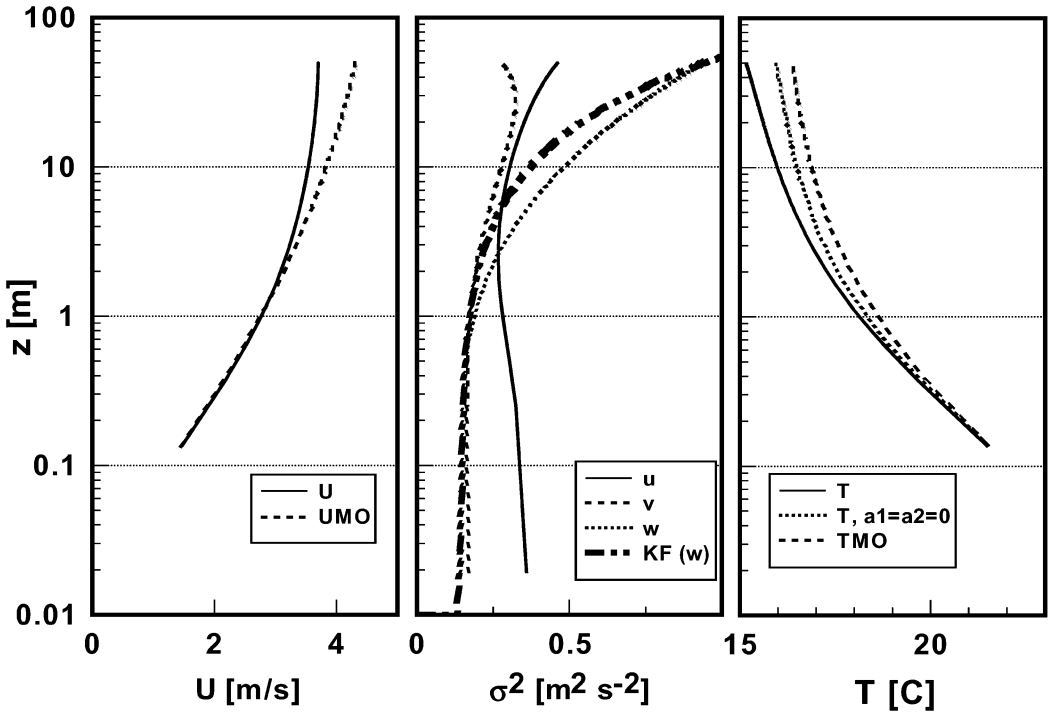

FIG. 4. Computed equilibrium profiles of mean velocity, velocity variance, and temperature, under unstable stratification ($u_* = 0.3$ m s^{-1}, $L = -9.1$ m) and with $\beta = 1°$. Also shown are Monin–Obukhov profiles [mean wind and temperature following Dyer and Bradley (1982); vertical velocity variance following Kaimal and Finnigan (1994, p. 16)] for the given conditions. Grid: $\Delta z = 0.25$ m, $z \leq 50$ m. Closure constants: $c_{\epsilon 1} = 1$, $c_{\epsilon 2} = 2$, $a_t = 0.15$, and $a_1 = 1/2$, $a_2 = -1/2$, or $a_1 = a_2 = 0$ (with negligible impact of this simplification on other profiles). The variance profiles are similar to the corresponding results of Bink (1996) and do not compare well to standard Monin–Obukhov curves.

scale) $k/\epsilon \propto z$, which in conjunction with feedbacks that assure height constancy of the stresses, results in $\partial/\partial z(U, V) \propto 1/z$.

Regarding the approach flow in simulations using LRR, as earlier mentioned this was simply imposed (i.e., not a numerical 1D solution). Equilibrium variances followed W85, that is, $c_{uu0} = 2.87$ and $c_{vv0} = c_{ww0} = 1.69$ implying $\sigma_{u,v,w}/u_* = (1.69, 1.3, 1.3)$ and $k/u_*^2 = 3.13$. The variance fields (in reality) are not invariant across neutral conditions, and, relative to the shear stresses, they do not (anyway) exert a strong influence on the mean velocity field. Thus, these differences (between the approach flows for the neutral RWC and the LRR simulations) are inconsequential.

One need have no hesitation in stating that, in the neutral case, the model fields far upwind from the windbreak fence are realistic.

b. RWC's stratified equilibrium (approach) flow

Figure 4 compares computed equilibrium profiles for a strongly stratified case ($L = -9$ m) with standard empirical Monin–Obukhov profiles. The distinction between the two modeled temperature profiles lies in the incorporation (or not) of a slight modification of the thermodynamic equations, in particular, the $\overline{T'^2}$ equation, by Bink (1996) and others earlier. Judging from the profiles shown, the original RWC closure is better in that its Monin–Obukhov (MO) function for temperature $\phi_T(z/L)$ is in better accord with that observed (though here it must be admitted that from the many field experiments, many ϕ_T functions have been proposed). Yet even so it seems warranted to complain that the RWC second-order closure produces Monin–Obukhov functions $\phi_u(z/L)$, $\phi_T(z/L)$, and $\phi_{uu}(z/L)$ for the mean wind, temperature, and variance that simply do not agree very well with the standard empirical functions. This is disappointing but not surprising (see Bink 1996, p. 113; Wilson et al. 2001). It raises the question, would it have been better to have used a different second-order closure?

One's immediate reaction is: probably not, because the closure assumptions of RWC are conventional, that is, common to the well-known closures. On the other hand, we have reports of successful simulations of the Monin–Obukhov functions by Lewellen and Teske (1973) and by Mellor (1973). Because this paper attempts to say something of generality on the usefulness of second-order RANS closures, the possibility that RWC is inferior needs to be pursued.

On close inspection one notes that on the unstable side, Mellor's ϕ_u does not agree well with observa-

tions—this would imply a divergence of his simulated U profile away from the MOST profile with increasing z/L, though the profile itself is not shown. On the other hand, Lewellen and Teske's computed profile for $\phi_u(z/L)$ is excellent over $-2 \leq z/L \leq 2$.

Lewellen and Teske used the second-order closure of Donaldson (1973), which features (i) Rotta-type isotropization terms representing pressure strain and analogous terms in scalar budget equations, introducing length scale Λ_1; (ii) a gradient-diffusion-type formulation for turbulent transport (length scale Λ_2) that has correct tensor symmetry (this distinction relative to the LRR and RWC closures used here is irrelevant to the point, for in the 1D case only the vertical gradient contributes); and (iii) explicit inclusion of diffusion terms representing pressure transport (with a third length scale Λ_3). Probably the crucial point distinguishing the Lewellen and Teske model is that it contains more optimizable coefficients (than the LRR and RWC closures used here), and that these were not prescribed wholly independent of the very data (MOST functions) the model was intended to reproduce.

The mediocre stratified-equilibrium profiles of the RWC closure (e.g., Fig. 4) must compromise the interpretation of the (following) assessment of whether these types of models have skill as regards the influence of stratification on disturbed flows. For in order to detect the influence of stability *experimentally*, large departures from neutrality are needed, to distinguish that influence from sampling (and other) errors in the measured data.[3] Yet far from neutrality the models themselves, even as regards the equilibrium flow, simply are not realistic.

4. Simulations of the Bradley–Mulhearn windbreak

Before looking at the Ellerslie observations it is warranted to revisit, and to some extent reinterpret, earlier simulations of the Bradley and Mulhearn (1983) fence (neutral, perpendicular winds; $h = 1.2$ m, $h/z_0 = 600$, $k_{r0} = 2$), a case which has played an important role in guiding the development of numerical shelter models. Figure 5 compares several computations with observed mean wind transects for that experiment. For each simulation the computational domain spans $-60 \leq x/h \leq 112$, $z/h \leq 47$ (''standard domain'' of W85), while the mesh was either the coarse, nonuniform ''standard grid'' of W85 with $\Delta x/h \geq 2$, $\Delta z/h \geq 0.25$, or a refined and uniform mesh $\Delta x/h = 1$, $\Delta z/h = 0.1$. On the standard grid, the present simulation with LRR closure reproduces the W85 result, the depth of the wind reduction

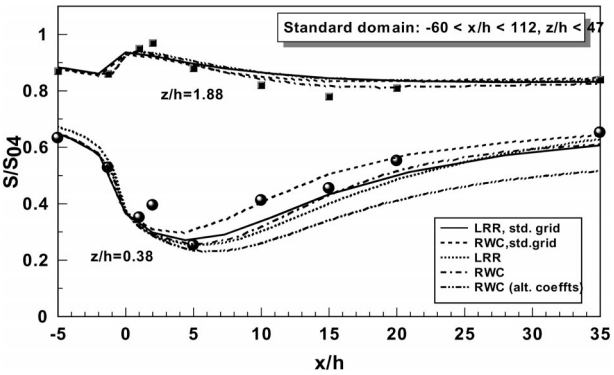

FIG. 5. Observed and computed relative wind speed S/S_{04} upwind and downwind from the Bradley–Mulhearn windbreak (neutral stratification, perpendicular approach wind; $h/z_0 = 600$, $k_{r0} = 2$) at $z/h = (0.38, 1.88)$; S_{04} is the mean wind speed at $z = 4$ m upwind from the windbreak. ''Standard grid'' refers to a particular, nonuniform and low-resolution grid used by W85; other simulations on refined uniform grid ($\Delta x/h = 1$, $\Delta z/h = 0.1$). RWC simulations ($c_{\epsilon 1} = 1$, $c_{\epsilon 2} = 2$); LRR simulations and ''RWC alt. coeffts,'' ($c_{\epsilon 1} = 1.44$, $c_{\epsilon 2} = 1.92$).

curve being roughly correct, but the recovery too slow. The RWC closure on the same (coarse, nonuniform) grid gave a shallower wind reduction curve but a better recovery; however, when resolution is refined, the distinction between the LRR and RWC simulations is unimportant. It is pertinent to emphasize that the data themselves are somewhat irregular, even though representing an average over about 25 h of near-neutral winds, and, consequently, it is difficult to argue for the superiority of one of these simulations over another (though in principle of course, the higher-resolution simulations are to be preferred).

On Fig. 5 RWC simulations are shown using both the choice ($c_{\epsilon 1} = 1.44$, $c_{\epsilon 2} = 1.92$) widely regarded as ''standard'' for the ϵ equation, and the choice ($c_{\epsilon 1} = 1$, $c_{\epsilon 2} = 2$) that has been usual with the RWC closure. The latter choice yields a markedly better outcome. Evidently on the refined grid there is little distinction between simulations with the RWC and the LRR closures, provided each is permitted the closure constants favored by its originators. Therefore, the main (and unsurprising) conclusion to be drawn from Fig. 5 is this: that discretization error (grid dependence), choice of closure, and specification of closure constants *all* to some extent affect the outcome of simulations of disturbed winds. W85's hypothesis that *all* RANS closures might give inadequate rate of recovery rested on the accident of the particular closures and grids he examined, and may be wrong;[4] although perhaps it is more useful to remark that, in view of the many choices to be made in RANS modeling, among these a choice will likely be possible in which the far wake *is* well simulated. The overall impression gained from comparisons like this is of an

[3] As Part I discusses, there are experimental pitfalls with the definition of extremely stratified cases too, in particular exacerbated overspeeding and possible stalling of cup anemometers, and the possibility of unwittingly having averaged across periods containing brief reversals of wind direction relative to the fence.

[4] But see Wilson and Mooney (1997), who argue from a perturbation analysis ($k_{r0} \to 0$) that eddy diffusion closures *do* underestimate the rate of recovery.

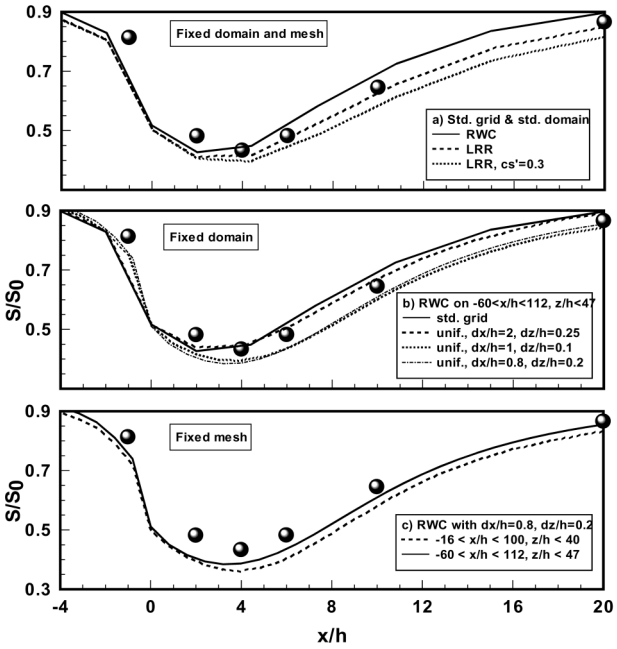

FIG. 6. Observed (solid symbols) and computed mean relative wind speed S/S_0 upwind and downwind from the Ellerslie fence ($h = 1.25$ m, $z_0 = 0.019$ m, $h/z_0 \sim 65$, and $k_{r0} = 2.4$), for neutral stratification and a perpendicular approach wind. (a) The RWC and LRR closures on the ''standard domain'' and nonuniform, low-resolution ''standard mesh'' of W85 (termed $D_s = [-60{:}112,\ 47]^{24}_{10,13}$) are compared. (b) Mesh (resolution) sensitivity of the RWC solutions on the standard domain, and (c) domain sensitivity on a uniform mesh. Each closure is here used with its favored coefficients, that is, for RWC $c_{\epsilon 1} = 1$, $c_{\epsilon 2} = 2$ and for LRR $c_{\epsilon 1} = 1.44$, $c_{\epsilon 2} = 1.92$.

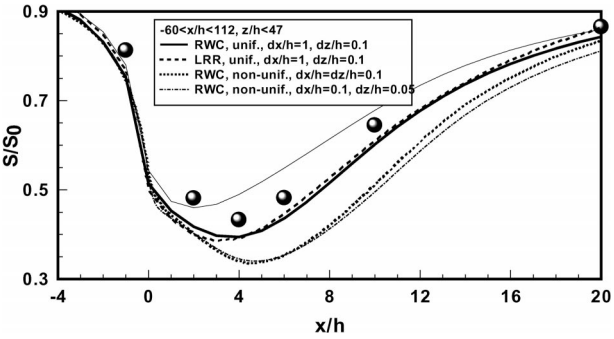

FIG. 7. RWC and LRR simulations on the standard domain and observations for neutral, perpendicular flow (Ellerslie experiment, $h = 1.25$ m, $z_0 = 0.019$ m, $h/z_0 \sim 65$, $k_{r0} = 2.4$). RWC and LRR are directly compared on uniform fine mesh ($dx/h = 1$, $dz/h = 0.1$), and RWC is also shown on a nonuniform mesh: $dx/h = 0.1$ ($|x/h| \leq 10$), and $dz/h = (0.1$ or $0.05)$ ($z/h \leq 4$). Outside the region of uniform fine mesh, grid length was gradually expanded to $dx/h = dz/h = 1$. The lighter solid line is the same simulation as the heavier solid line (RWC with uniform mesh), but the model's cup wind speed has been evaluated using Eq. (47) in full (variance terms retained). Each closure was used with its favored coefficients.

ambiguity in the modeling enterprise; but we should not lose sight of the sampling error in individual 15-min experimental transects, which may not be much smaller that the (very roughly) 10%–15% ambiguity in the amplitude ($\Delta S/S_0$ at the location $\check{x}$ of minimum wind speed) of the modeled wind reduction curves evidenced by Fig. 5.

5. Simulations of the Ellerslie windbreak

For the Ellerslie simulations, $h = 1.25$ m, $z_0 = 0.019$ m ($h/z_0 = 65$), and, unless otherwise specified, $k_{r0} = 2.4$. Regarding the observations, it is to be recalled that the reference mean wind speed S_0 is that observed in the approach flow at $z = 0.62$ m $= h/2$ and that data from periods with $S_0 < 1$ m s^{-1} have been rejected (other selection criteria are given in Part I).

a. Neutral winds at perpendicular incidence

The upper panel of Fig. 6 indicates that simulations of the Ellerslie experiment on the ''standard grid'' of W85 are fairly compatible with the observations, irrespective of which of the two closures one picks. This close similarity of outcomes is unsurprising, in view of the close similarity of the two closures, but note the proviso that it depends on each being implemented with the values of the coefficients recommended by the original authors, namely for the RWC simulations $c_{\epsilon 1} = 1$, $c_{\epsilon 2} = 2$, and for the LRR simulations $c_{\epsilon 1} = 1.44$, $c_{\epsilon 2} = 1.92$, and $c_s' = 0.25$ ($\neq 2a_t$). The middle and lower panels of Fig. 6, respectively, illustrate sensitivity of RWC simulations to resolution (with fixed domain) and domain size (with fixed, uniform resolution); these emphasize the necessity for a high resolution over a very large domain.

Figure 7 directly compares simulations using the RWC and LRR closures on the refined, uniform grid ($\Delta x/h = 1$, $\Delta z/h = 0.1$). The computed transects are very similar and slightly overestimate mean wind reduction. Also given on Fig. 7 are comparative RWC simulations on two nonuniform meshes covering the same (''standard'') domain, with computational resolution in the region $|x/h| \leq 10$, $z/h \leq 4$ refined to ($dx/h = dz/h = 0.1$) or ($dx/h = 0.1$, $dz/h = 0.05$). Outside of this region, the grid lengths were stretched from cell to cell by a constant factor of 20%. Stopping criteria for both runs were the same, but the iteration count was much larger for the $dz/h = 0.05$ run, and conceivably the distinction in outcomes relates to that factor, not the finer grid. What Figs. 6 and 7 indicate is the difficulty of deciding how fine the computational resolution needs to be to ensure grid independence (and there is no reason to suppose it has been obtained even with $dx/h \sim dz/h \sim 0.1$). Among simulations with differing uniform and nonuniform meshes it is difficult to discern systematic influences. However, it is plain that the computed wind reduction curve is systematically deepened as computational resolution is improved, such that the low-resolution simulations of W85 happily but fortuitously give best agreement with observations,

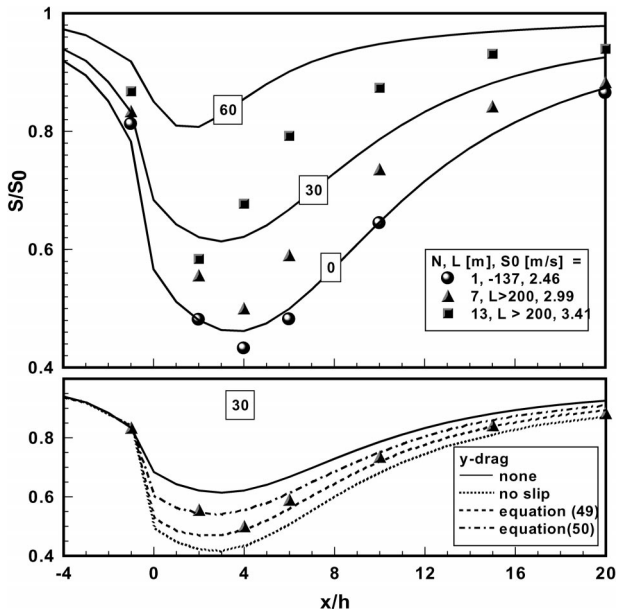

FIG. 8. Observed and computed transects of relative wind speed versus orientation of the upwind flow (neutral stratification). Legend indicates the number of 15-min periods compounded, the stability class, and the mean approach wind speed; symbols distinguish the orientations as $\beta = 0$ (filled circle), $\beta = 30°$ (filled triangle), and $\beta = 60°$ (filled square). The simulations shown (solid lines) stem from the RWC closure on the refined grid, with $c_{\epsilon 1} = 1$, $c_{\epsilon 2} = 2$, and $k_{r0} = 1.8$, intentionally reduced from the correct value ($k_{r0} = 2.4$) to "tune" the $\beta = 0$ simulation to match the perpendicular transect. The lower panel explores consequences of several treatments of drag in the V momentum equation (neglected in all other simulations).

when using the value of the resistance coefficient k_{r0} determined in the wind tunnel (i.e., $k_{r0} = 2$ for the Bradley–Mulhearn experiment, and $k_{r0} = 2.4$ for the Ellerslie experiment).

Figure 7 also addresses the significance of the inclusion of the terms in velocity variance when the model's cup wind speed is estimated using Eq. (47), instead of the simpler (but, in principle, less legitimate) $S = \sqrt{\overline{u}^2 + \overline{v}^2}$. Because (as shown in section 5d) the models compute a large rise in the velocity variances in the lee of the barrier, inclusion of these terms substantially alters the models' relative mean wind speed curves. The simpler estimate $S = \sqrt{\overline{u}^2 + \overline{v}^2}$ gives what seems a more reasonable result.

b. Neutral winds at oblique incidence

Having seen that for the perpendicular case reasonably good wind reduction curves are given by the RANS models, though with a troubling level of ambiguity (about 10%–15% of the amplitude of the relative wind curve) linked primarily to discretization error, it is of interest to see whether RANS computes equally well the consequences of obliquity of the wind. Figure 8 gives observed wind reduction curves for $\beta = 0°$, 30°, and 60°, in comparison with computations using the RWC closure, with $c_{\epsilon 1} = 1$, $c_{\epsilon 1} = 2$. Here in the simulations a uniform mesh ($dx/h = 0.1$, $dz/h = 0.1$) covers the standard domain ($-60 \le x/h \le 112$, $z/h \le 47$), and k_{r0} has been deliberately reduced to $k_{r0} = 1.8$ (from the correct value $k_{r0} = 2.4$) to better match the $\beta = 0$ simulation to the observations.

The computations are qualitatively consistent with the observations in the sense that obliquity systematically reduces shelter[5] in the near lee, and moves the point of minimum wind speed closer to the windbreak. However computed *differences* between the relative winds at a given location for the cases $\beta = 0$, 30, and 60° are much greater than the differences observed, such that the model underestimates shelter from oblique winds. Could this be because it has been *assumed* that the fence does not remove V momentum, that is, $\overline{f}_y = 0$? The assumption is without consequence as far as the simulations of perpendicular flow are concerned, but has a direct bearing on the oblique cases. The lower panel of Fig. 8 shows the impact of alternative treatments in which either the parallel component has been required to vanish at the fence ("no slip"), or a localized momentum sink has been inserted in the V momentum equation, either

$$\overline{f}_y = -k_{r0} V \sqrt{U^2 + V^2}\, \delta(x - 0) s(z - h) \quad \text{or} \tag{49}$$

$$\overline{f}_y = -[U(x^-, z)V(x^-, z) - U(x^+, z)V(x^+, z)] \times \delta(x - 0) s(z - h). \tag{50}$$

Equation (49) parallels the step one would take were the windbreak made up of a finite width of plants or trees, in which case k_{r0} would be the product $C_d AX$ of a drag coefficient C_d with the foliage area density A and width X of the shelter. Equation (50), implemented with $x^{\pm} = x \pm \Delta x/2$ (and entailing linear interpolation between the grid points at the fence and immediately upstream and downstream), approximates Eq. (11). These treatments of the influence of the fence in the V momentum equation ("parallel drag") cover a range of plausible possibilities; none altered the computed solutions in a definitively favorable way, relative to the observations (an ensemble average over seven cases). Therefore, although in assessing the performance of the RANS wind models one needs to bear in mind that the interaction of the fence and the flow has been parametrized, it seems unlikely that mere refinement of that parameterization will bring the steady-state RANS approach into substantially better accord with observations, as regards the effect of obliquity. A plane windbreak fence has something of the character of a wing, and so perhaps it may be unsurprising that the vortex dynamics (that are *implicit* in a RANS closure, and tuned to the reference flow) should fail to properly model the

[5] Computations by Wang and Takle (1996) using first-order closure for a shelterbelt of thickness $h/2$ indicated an *enhanced* shelter in the near lee in oblique winds, though only for "low density" windbreaks. No such effect was reported by Nord (1991) in her observations around tree windbreaks.

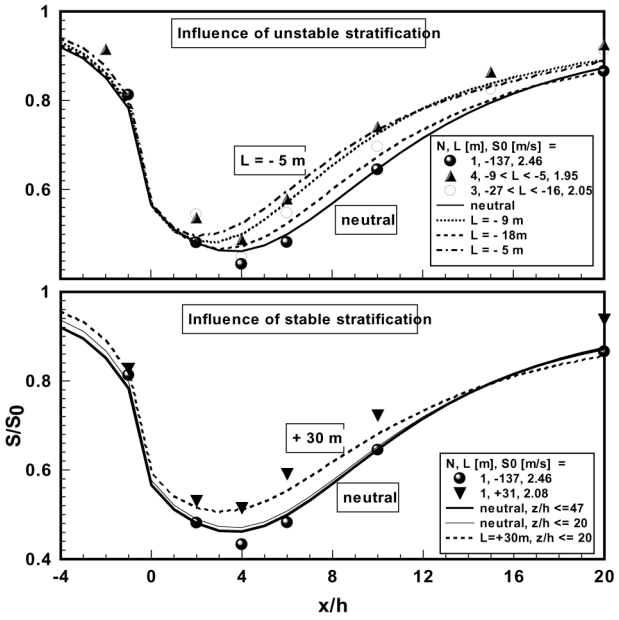

FIG. 9. Observed (solid symbols) and computed stability dependence of the mean relative wind speed around the Ellerslie fence, for a perpendicular approach wind. Simulations using the RWC closure on a uniform mesh ($dx/h = 0.1$, $dz/h = 0.1$), with the resistance coefficient ''tuned'' so that the neutral simulation (solid line) matches the observations ($k_{r0} = 1.8$). (top) Cases of unstable stratification (upstream Obukhov length $L = -18$, -9, and -5 m) computed on the standard domain; (bottom) case of stable stratification, computed on a shallower domain.

response of the mean flow to this varying ''angle of attack.''

c. Stratified winds at perpendicular incidence

The upper panel of Fig. 9 compares the observed influence of unstable thermal stratification in the case of winds at perpendicular incidence, with that indicated by simulations using RWC (with $c_{\epsilon 1} = 1$, $c_{\epsilon 2} = 2$) on the standard domain and with the uniform grid ($dx/h = 1$, $dz/h = 0.1$). Of course these solutions are not grid independent, and the resistance coefficient has (again) been tuned away from its proper value so that the neutral simulation matches the observations (one might say the wind model is being used in a ''differential mode''). The influence of stratification is (correctly, it appears from the limited data) computed to be restricted to the leeward side of the fence. Furthermore, the simulations are qualitatively consistent with the observation that unstable stratification compromises (reduces) shelter and shifts the point $\check{x}$ of lowest mean wind speed closer to the fence.

For stable stratification (lower panel of Fig. 9), and particularly if the magnitude of the Obukhov length is small, a compromise has to be reached between the conflicting requirements of a deep computational domain, and the validity of the 1D (equilibrium) profile solutions, which entails retaining z/L small enough (say, less than unity) on the entire height axis. For the simulation of even a modestly stable case ($L = +30$ m), it was found to be necessary to reduce the height of the domain from $z/h = 47$ to $z/h = 20$. To eliminate any possibility of being confounded as regards the modeled influence of stability by comparing neutral and stable runs computed on different domains, that is, to properly use the numerical model in a differential mode, the neutral case was rerun on the same domain; as shown, the two outcomes for $L = \infty$ are hardly distinguishable. The comparative RWC solutions for $L = \infty$, $+30$ m are consistent with the observations, in that stable stratification (like unstable) results in a shallower relative wind curve (reduced wind protection). Not forgetting that k_{r0} has been tuned away from its proper value for these simulations or forgetting the arbitrariness of using this particular mesh, one can credit the RWC solution with providing something like the correct stratification response, in the near lee. This conclusion does not rest on a specific choice of the solution mesh, for other computations (not shown) on the standard domain and using the coarser, nonuniform ''standard grid'' of W85 were about equally consistent with the observations.

d. Computed ''quiet zone'' for neutral, perpendicular winds

Figure 10 shows that RANS simulations using the RWC (or LRR) closure do produce some semblance of the expected quiet zone in the near lee, and that this quiet zone is more marked in σ_u than in σ_v (recall there is no sink for σ_v^2 at the fence; probably the sudden dip in σ_v in the immediate lee reflects redistribution loss of energy to σ_u^2, which in contrast according to the present treatment *is* directly ''filtered'' at the fence). Overall, however, the simulations of the velocity standard deviations compare poorly with the observations, in particular as regards the poorly estimated span of the quiet zone, and (computed) region of markedly more energetic turbulence away from the immediate lee. There is, however, reason to be guarded about the observations. Enhanced shear in the region $z/h \gtrsim 1$ has in other experiments been observed to result in a turbulent wake spreading from the tip of the windbreak (Raine and Stevenson 1977; Finnigan and Bradley 1983; Wilson 1987; McNaughton 1989), and so in fact the Ellerslie observations, provided by a sparse transect along $z/h = 1/2$ of two-dimensional sonic anemometers at $x/h = (-12, 4, 10, 15)$, are surprising as regards the lack of evidence of that zone (i.e., for the neutral, perpendicular case the σ_u transect shows no influence whatsoever of the supposed turbulent wake zone, while the σ_v transect shows only about a 10% rise over the upstream level).

In any case the simulations do not predict the extended quiet zone observed in σ_u, computing instead a very rapid (over) recovery. Given that the mean flow is simulated reasonably well, suspicion must fall on the parameterized terms in the σ_u^2 budget [Eq. (24)], par-

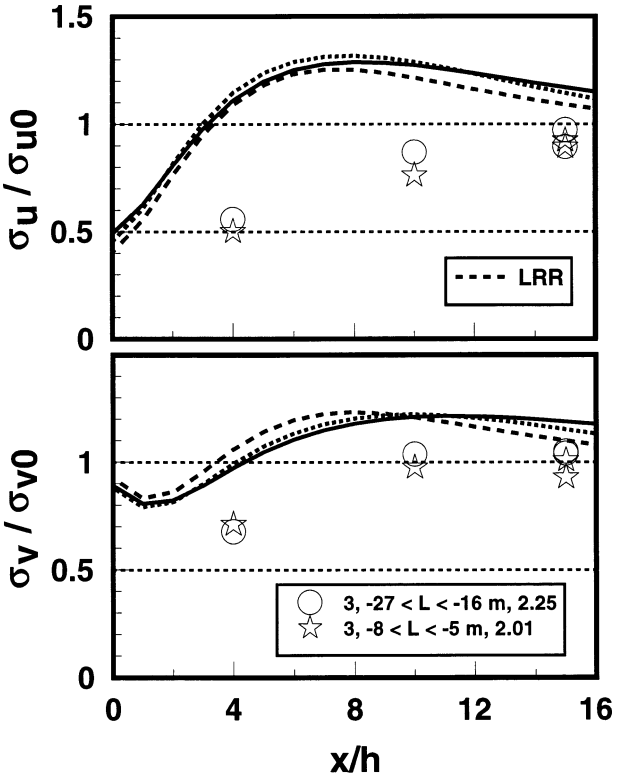

FIG. 10. Observed (symbols) and computed transects of the normalized standard deviations $\sigma_{u,v}(x, h/2)/\sigma_{u,v}(-\infty, h/2)$ RWC simulation with $k_{r0} = 1.8$ (solid line), RWC with $k_{r0} = 2.4$ (short-dashed line), and LRR with $k_{r0} = 1.8$ (long-dashed line).

ticularly the closures for turbulent and pressure transport (represented by diffusion terms), for redistribution (the LRR and RWC differ in an essential way only here; RWC contains the Rotta-type isotropization term, alone), and for the dissipation rate ϵ. This failure of the RANS wind models to predict a satisfactory field of the turbulent velocity variances is disappointing. It would be useful (e.g., in the context of urban dispersion models) to be able to (rapidly) compute a field of the flow properties U_i, $\overline{u_i' u_j'}$, ϵ, which are the key inputs to ''drive'' the Lagrangian stochastic class of dispersion models.

6. Conclusions

Whatever the quality of these RANS simulations of windbreak flow, the exercise deserves the following credits. Only after the comparison with models had begun did the author cease joining the experimental data points at $x/h = (-1, +2)$ with line segments, which inappropriately averaged the highly variable intermediate slope evident from the models (in hindsight, this was the most elementary of errors). Second, early drafts of graphs of Part I included observations at $x/h = -2$ that compared woefully with the simulations (notice the ''band'' of model results is far narrower upwind than in the lee); on closer examination these could justifiably be omitted, because a single cup anemometer had covered both positions $x/h = -2, -1$, and these outliers owed to a single 15-min interval, whereas observations at greater x/h represented a more satisfactory average. Thus, RANS simulations can play a useful guiding role in the analysis of observations.

From the present simulations and those of Wilson and Yee (2003), it seems necessary to admit that the RANS approach to shelter flows produces not a single curve for comparison with observed transects or profiles, but a *band.* This ambiguity stems minimally from choice of closure (though only two, and very similar, closures were tested here), and, more important, from discretization error, whose elimination, if even possible in practice, will require a mesh much finer than that used in these simulations. There seems no call to be excessively troubled by this looseness in what we consider the computational flow field, when we recall that the sampling error in single-run observational statistics of very disturbed atmospheric flows is comparably large. What has been demonstrated is that notwithstanding the nonuniqueness of ''the'' RANS solution (across differing closures, closure coefficients, domain, and mesh), provided one is careful to keep constant all aspects of the simulation except the obliquity (β) or stratification (L) of the upwind flow, then the computed responses of the mean wind transect to variations in β, L are correct, at the *qualitative* level. However, if one demands *quantitative* skill, then the computed response of the mean wind speed transect to obliquity must be said to be poor; even for normally incident winds, the computed transects of velocity variance are unacceptable. May one draw the conclusion, of some significance for the application of RANS in environmental analysis and assessment, that these models do not objectively capture reality[6] in a world of complex boundaries and high Reynolds numbers? If so, then it will be necessary to refine the closure approximations, and (though this is probably of significance only close to unresolved boundaries) to assess the legitimacy of neglecting the component $\langle \overline{u_i'' u_j''} \rangle$ of the compound Reynolds stress that emerges from the joint time–volume averaging.

Do these indications as to the limited capability of RANS rest on the fact that the closures examined date from the 1970s? Subsequent developments in steady-state RANS closures at second order have mainly targeted improved prediction very near boundaries, where Eq. (44) for the influence of pressure fluctuations is known to be invalid. Greatly improved computing power and better parameterization of the near-wall flow obviate the need to use ''wall functions,'' which presuppose (adjacent to boundaries) an equilibrium structure that may be illegitimate. Substitution (Durbin 1991,

[6] It is pertinent that engineers and CFD specialists now regard RANS as inadequate for separating and reattaching turbulent flows (e.g., Keating et al. 2004, section 1).

1993) of a differential equation in lieu of an algebraic equation [like Eq. (44)] for the redistribution tensor is found (e.g., Manceau and Hanjalic 2000) to improve the prediction of mean velocity and shear stress profiles in the ''buffer layer'' just outside the viscous sublayer. However, such developments of the closure assumptions seem unlikely to greatly impact and improve computations of micrometeorological winds, that is, flows over fully aerodynamically rough surfaces, for these reasons: first, and as direct evidence, W85 found that incorporation of a near-wall correction to the pressure strain, and of alternatives to the simple-minded wall functions, had no valuable impact on the quality of windbreak simulations; second, and more broadly, in micrometeorology we seldom make measurements so close to ground that the turbulence approaches two-dimensionality, that is, we do not even hope to resolve and describe the equivalent of the viscous and buffer layers adjacent to the metal surfaces of ducts and channels.

Two factors recommend that the present diagnosis of the fundamental competence of RANS be interpreted as provisional: has the unresolvable aerodynamic effect of the barrier been properly represented by the momentum sinks? And what of the impact of discretization errors, that is, faulty numerical procedure? Launder (1989) holds improvements in discretization schemes and refined grids as at least partly responsible for the emergence of a definite edge of second-order over *K*-closures, and certainly discretization error plagues the effort to determine the merits of the various closure models. Even the finest grid used here ($\Delta x/h = \Delta z/h = 1/10$, i.e., $\Delta x = \Delta z \sim 10$ cm) is coarse relative to the thickness of the fence, and it may be that ''smoothing out'' rapid changes in wind direction that occur very close to a barrier is problematical. In principle, discretization error reflects careless work, and *simply should not be there*; but if one is unwilling to look at numerical solutions that contain discretization error, then one is unwilling to look at numerical solutions. Grid independence cannot easily be established, and owing to the rapid changes in wind direction near a porous barrier it conceivably might not be attainable unless the mesh is refined to Δx, $\Delta z \sim d_x$ (where $d_x \sim 1$ mm is the thickness of the fence). By using a nonuniform grid, converged simulations with $\Delta x/h = 0.1$ in the region of the barrier were obtained. However, although they differed from the simulations on the coarser uniform grid, they were not themselves grid independent. It may be fair to say that a law of diminishing returns sets in while attempting to refine the mesh.

It is an interesting observation that sometimes numerical convergence for the windbreak flow could not be attained using these steady-state RANS models: is this a hint that the assumption of steady state is dubious, and that possibly the equations are being driven in ''search of a solution that might not exist'' (Castro et al. 2003)? Unsteady vortex shedding by a fence perhaps makes such a flow a candidate for unsteady RANS (URANS) simulations, in which one computes explicitly the largest eddies while burying smaller eddies in the averaging, an approach that has been explored for ''unsteady'' turbulent flows about buildings or idealized bluff bodies (Gosman 1999; Lübcke et al. 2001) and over hills (Castro et al. 2003). Anyone who has observed the vortices that bend the grass and roll downwind in the lee of a windbreak is likely to consider time-dependent simulation (URANS or LES) as a fascinating idea, notwithstanding that the spectral division (resolved/unresolved) in URANS is generally ambiguous (*all* turbulent flows are unsteady, and at high Reynolds numbers no convenient spectral gap permits spectral division) and the arbitrary designation of a certain class of flows as *peculiarly* unsteady is problematical in principle. For now, one may only speculate whether URANS may hold an advantage over RANS; and certainly there is nothing in principle that prevents windbreak flows from being treated as steady-state, and modeled using RANS, provided averages are suitably formed. However, ''success'' in science (or ''theoretical modeling'') may well depend on what patterns one chooses to create, to describe, and to theorize about: the choice (here) to describe windbreak flow by averaging for 15 min to define a (posited) steady state may have thrown up a pattern that is as difficult to model as it is unrepresentative of the instantaneous reality.

To conclude, it would be excessively cynical to say that RANS models are no more than complex and ambiguous algorithms to draw curves on graphs of observations.[7] It would be excessively naive to say that they objectively describe the real world. Experimentalists may tend toward the first of these extreme views, while occasionally protagonists of models may err toward the other (one should reiterate the point that what one chooses to call ''experimental reality'' is also to some extent a matter of taste). Probably the balanced view is to reassert the *potential* value of RANS wind models, to continue testing new closures as well as schemes that reduce discretization error, and—wherever the issue of their *absolute correctness* matters—to avoid their premature employment as a substitute for measurements, however onerous the latter may be.

Acknowledgments. This work has been supported by research grants from the Natural Sciences and Engineering Research Council of Canada (NSERC) and the Canadian Foundation for Climate and Atmospheric Sciences (CFCAS). The author thanks Drs. Keith Hage and Gerhard Reuter, as well as the three anonymous reviewers, for their constructive comments.

[7] It is literally true that the *function* of RANS models is no more than the provision of smooth curves (having a rational basis, viz. satisfying the conservation principles) of the variation of flow statistics across the domain, guided by measured (or supposed) boundary values.

REFERENCES

Bink, N. J., 1996: The structure of the atmospheric surface layer subject to local advection. Ph.D. thesis, Wageningen Agricultural University, 206 pp.

Bradley, E. F., and P. J. Mulhearn, 1983: Development of velocity and shear stress distributions in the wake of a porous shelter fence. *J. Wind Eng. Indust. Aerodyn.,* **15,** 145–156.

Castro, F. A., J. M. L. M. Palma, and A. S. Lopes, 2003: Simulation of the Askervein flow part 1: Reynolds averaged Navier–Stokes equations (k–ϵ turbulence model). *Bound.-Layer Meteor.,* **107,** 501–530.

Daly, B. J., and F. H. Harlow, 1970: Transport equations in turbulence. *Phys. Fluids,* **13,** 2634–2649.

Donaldson, C., 1973: Construction of a dynamic model of the production of atmospheric turbulence and the dispersal of atmospheric pollutants. *Workshop on Micrometeorology,* D. A. Haugen, Ed., Amer. Meteor. Soc., 313–392.

Durbin, P. A., 1991: Near-wall turbulence closure modeling without 'damping functions.' *Theor. Comput. Fluid Dyn.,* **3,** 1–13.

——, 1993: A Reynolds stress model for near-wall turbulence. *J. Fluid Mech.,* **249,** 465–498.

Dyer, A. J., and E. F. Bradley, 1982: An alternative analysis of flux-gradient relationships at the 1976 ITCE. *Bound.-Layer Meteor.,* **22,** 3–19.

Finnigan, J. J., 1985: Turbulent transport in flexible plant canopies. *The Forest-Atmosphere Interaction,* B. A. Hutchison and B. B. Hicks, Eds., D. Reidel, 443–480.

——, and E. F. Bradley, 1983: The turbulent kinetic energy budget behind a porous barrier: An analysis in streamline co-ordinates. *J. Wind Eng. Ind. Aerodyn.,* **15,** 157–168.

Gosman, A. D., 1999: Developments in CFD for industrial and environmental applications in wind engineering. *J. Wind Eng. Ind. Aerodyn.,* **81,** 21–39.

Green, S. R., 1992: Modelling turbulent air flow in a stand of widely spaced trees. *Phoenics J.,* **5,** 294–312.

——, N. Hutchings, and J. Grace, 1994: Modelling turbulent airflow in sparse tree canopies. Preprints, *21st Conf. on Agricultural and Forest Meteorology,* San Diego, CA, Amer. Meteor. Soc., 86–87.

Kaimal, J. C., and J. J. Finnigan, 1994: *Atmospheric Boundary Layer Flows.* Oxford University Press, 289 pp.

Keating, A., U. Piomelli, K. Bremhorst, and S. Nesic, 2004: Large-eddy simulation of heat transfer downstream of a backward-facing step. *J. Turbulence,* **5,** 020, doi:10.1088/1468-5248/5/1/020.

Launder, B. E., 1989: Second-moment closure: Present and future? *Int. J. Heat Fluid Flow,* **10,** 282–300.

——, G. J. Reece, and W. Rodi, 1975: Progress in the development of a Reynolds-stress turbulence closure. *J. Fluid Mech.,* **68,** 537–566.

Laws, E. M., and J. L. Livesey, 1978: Flow through screens. *Annu. Rev. Fluid Mech.,* **10,** 247–266.

Lewellen, W. S., and M. Teske, 1973: Prediction of the Monin–Obukhov similarity functions from an invariant model of turbulence. *J. Atmos. Sci.,* **30,** 1340–1345.

Lien, F. S., E. Yee, and J. D. Wilson, 2004: Numerical modelling of the turbulent flow developing within and over a 3-d building array, part II: A mathematical foundation for a distributed drag force approach. *Bound.-Layer Meteor.,* in press.

Lübcke, H., S. Schmidt, T. Rung, and F. Theile, 2001: Comparison of LES and RANS in bluff-body flows. *J. Wind Eng. Ind. Aerodyn.,* **89,** 1471–1485.

Lumley, J. L., 1979: Prediction methods for turbulent flows. von Karman Institute for Fluid Dynamics Lecture Series 1979-2, Rhode-Saint-Genese, 26 pp.

——, and B. Khajeh-Nouri, 1974: Computational modeling of turbulent transport. *Advances in Geophysics,* Vol. 18A, Academic Press, 169–192.

Manceau, R., and K. Hanjalic, 2000: A new form of the elliptic relaxation equation to account for wall effects in RANS modeling. *Phys. Fluids,* **12,** 2345–2351.

McNaughton, K. G., 1989: Micrometeorology of shelterbelts and forest edges. *Philos. Trans. Roy. Soc. London,* **B324,** 351–368.

Mellor, G. L., 1973: Analytic prediction of the properties of stratified planetary surface layers. *J. Atmos. Sci.,* **30,** 1061–1069.

Miguel, A. F., N. J. van de Braak, A. M. Silva, and G. P. A. Bot, 2001: Wind-induced airflow through permeable materials part 1: the motion equation. *J. Wind Eng. Ind. Aerodyn.,* **89,** 45–57.

Nord, M., 1991: Shelter effects of vegetation belts—Results of field measurements. *Bound.-Layer Meteor.,* **54,** 363–385.

Raine, J. K., and D. C. Stevenson, 1977: Wind protection by model fences in a simulated atmospheric boundary layer. *J. Wind Ind. Aerodyn.,* **2,** 159–180.

Rao, K. S., J. C. Wyngaard, and O. R. Cote, 1974a: Local advection of momentum, heat, and moisture in micrometeorology. *Bound.-Layer Meteor.,* **7,** 331–348.

——, ——, and ——, 1974b: The structure of the two-dimensional internal boundary layer over a sudden change of surface roughness. *J. Atmos. Sci.,* **31,** 738–746.

Raupach, M. R., and R. H. Shaw, 1982: Averaging procedures for flow within vegetation canopies. *Bound.-Layer Meteor.,* **22,** 79–90.

Taylor, G. I., and G. K. Batchelor, 1949: The effect of wire gauze on small disturbances in a uniform stream. *Quart. J. Mech. Appl. Math.,* **2,** 1–29.

Wang, H., and E. S. Takle, 1995a: Boundary-layer flow and turbulence near porous obstacles: I derivation of a general equation set for a porous media. *Bound.-Layer Meteor.,* **74,** 73–88.

——, and ——, 1995b: A numerical simulation of boundary-layer flows near shelterbelts. *Bound.-Layer Meteor.,* **75,** 141–173.

——, and ——, 1996: On shelter efficiency of shelterbelts in oblique winds. *Agric. For. Meteor.,* **81,** 95–117.

Wilson, J. D., 1985: Numerical studies of flow through a windbreak. *J. Wind Eng. Ind. Aerodyn.,* **21,** 119–154.

——, 1987: On the choice of a windbreak porosity profile. *Bound.-Layer Meteor.,* **38,** 37–49.

——, 1988: A second-order closure model for flow through vegetation. *Bound.-Layer Meteor.,* **42,** 371–392.

——, 2004: Oblique, stratified winds about a shelter fence. Part I: Measurements. *J. Appl. Meteor.,* **43,** 1149–1167.

——, and C. J. Mooney, 1997: Comments on ''A numerical simulation of boundary-layer flows near shelterbelts'' by H. Wang and E. Takle. *Bound.-Layer Meteor.,* **85,** 137–149.

——, and T. K. Flesch, 2003: Wind measurements in a square plot enclosed by a shelter fence. *Bound.-Layer Meteor.,* **109,** 191–224.

——, and E. Yee, 2003: Calculation of winds disturbed by an array of fences. *Agric. For. Meteor.,* **115,** 31–50.

——, T. K. Flesch, and L. A. Harper, 2001: Micro-meteorological methods for estimating surface exchange with a disturbed windflow. *Agric. For. Meteor.,* **107,** 207–225.

Wilson, N. R. and R. H. Shaw, 1977: A higher-order closure model for canopy flow. *J. Appl. Meteor.,* **16,** 1197–1205.